**Table 1.** Dendritic protrusion density and size (Mean±SEM) in hippocampal CA1 neurons

| | Density (number/10 μm) | | | Length of protrusion (μm) | Width of protrusion (μm) |
|---|---|---|---|---|---|
| | Protrusions | Spines | Filopodia | | |
| Wild-type (P14) | 6.68±0.20 | 5.04±0.04 (75.6±2.1%) | 1.64±0.19 (24.4±2.1%) | 1.25±0.03 | 0.73±0.02 |
| GlcAT-P −/− (P14) | 6.81±0.25 | 2.97±0.01 (43.7±1.8%) | 3.84±0.26 (56.3±1.8%) | 1.71±0.02 | 0.64±0.01 |
| Wild-type (adult) | 12.29±0.68 | 11.23±0.50 (91.5±1.0%) | 1.06±0.18 (8.5±1.0%) | 1.05±0.03 | 0.71±0.02 |
| GlcAT-P −/− (adult) | 10.46±0.57 | 8.72±0.59 (83.8±6.8%) | 1.74±0.81 (16.2±6.8%) | 1.17±0.01 | 0.69±0.02 |

and 96.4% of the wild-type values, respectively (Fig. 2B, Table 2). In addition, the proportion of mature spines increased to 78.6±2.2%, which was comparable to the 75.8±1.5% found in wild-type neurons (Fig. 2C, Table 2, $P$=0.48). This result indicates that the spine morphology in GlcAT-P-deficient neurons can be mostly restored by HNK-1 expression during the later stage of spine maturation (15 to 18 DIV) in spite of the absence of HNK-1 until 15 DIV.

### Loss of the HNK-1 epitope facilitates dendritic accumulation of postsynaptic proteins and shaft synapse formation

Next, to examine whether the absence of HNK-1 had an effect on synapse formation, neurons at 19 DIV were doubly immunostained for PSD-95 (postsynaptic marker protein) and synaptophysin (presynaptic marker protein). In both wild-type and GlcAT-P-deficient neurons, these proteins were clustered and closely apposed to each other, indicating that functional synapses were formed (Fig. 4A). Quantitative analysis revealed that there were no significant differences in the densities of either PSD-95 clusters (Fig. 4B, left) or synapses marked by PSD-95 and synaptophysin clustering (Fig. 4B, right) between wild-type and GlcAT-P-deficient neurons. However, the synapses that formed in GlcAT-P-deficient neurons were localized much more abundantly along dendritic shafts or the dendritic periphery (Fig. 4A, arrows), rather than on spine heads (Fig. 4A, arrowheads). These results indicated that the

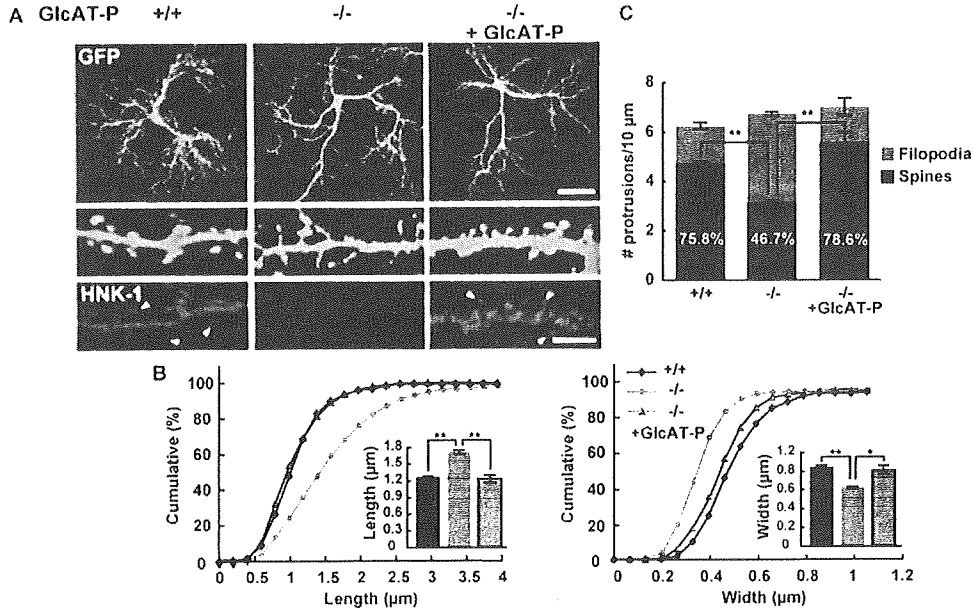


Fig. 2. Impaired spine morphology of cultured GlcAT-P −/− hippocampal neurons. (A) Cultured hippocampal neurons were transfected with GFP alone (left and middle) or GFP plus GlcAT-P (right) at 15 DIV and were then double immunostained for GFP (green) and HNK-1 (red) at 18 DIV. Higher magnification panels show individual dendrite segments. Arrowheads indicate HNK-1 staining on the dendritic spines. Scale bars: 50 μm in the upper panel and 5 μm in the lower panel. (B) Cumulative frequency plots of the length and width of protrusions ($n$=916 for wild-type neurons; $n$=933 for GlcAT-P −/− neurons; $n$=923 for GlcAT-P −/− neurons rescued with GlcAT-P). $P$<0.01 (Kolmogorov–Smirnov Test). Inset histograms show mean values ($n$=4, 197–231 protrusions per experiment for wild-type neurons; $n$=4, 189–216 protrusions per experiment for GlcAT-P −/− neurons; $n$=5, 153–196 protrusions per experiment for GlcAT-P −/− neurons rescued with GlcAT-P). * $P$<0.05, ** $P$<0.01 (two-tailed $t$-test). (C) The densities of protrusions in (B) ($n$=4, 9–10 cells per experiment for wild-type neurons; $n$=4, 9–10 cells per experiment for GlcAT-P −/− neurons; $n$=5, 6–10 cells per experiment for GlcAT-P −/− neurons rescued with GlcAT-P). The numbers on the bars indicate the percentages of mature spines within all protrusions. ** $P$<0.01 (two-tailed $t$-test). Error bars indicate SEM.

**Table 2.** Dendritic protrusion density and size in cultured hippocampal neurons

| | Density (number/10 μm) | | | Length of protrusion (μm) | Width of protrusion (μm) |
|---|---|---|---|---|---|
| | Protrusions | Spines | Filopodia | | |
| Wild-type (WT) 18 DIV | 6.23±0.11 | 4.71±0.09 (75.8±1.5%) | 1.52±0.11 (24.2±1.5%) | 1.28±0.01 | 0.84±0.02 |
| GlcAT-P −/− (KO) 18 DIV | 6.72±0.04 | 3.14±0.08 (46.7±1.3%) | 3.58±0.10 (53.3±1.3%) | 1.71±0.04 | 0.63±0.01 |
| KO+GlcAT-P | 6.99±0.37 | 5.52±0.46 (78.6±2.2%) | 1.47±0.18 (21.4±2.2%) | 1.25±0.05 | 0.77±0.01 |
| WT 12 DIV | 4.14±0.06 | | | 3.23±0.22 | |
| KO 12 DIV | 4.35±0.27 | | | 3.20±0.12 | |
| WT+GluR2 | 7.38±0.19 | 6.86±0.17 (93.0±1.3%) | 0.52±0.10 (7.0±1.3%) | 1.43±0.03 | 1.04±0.01 |
| KO+GluR2 | 6.50±0.21 | 6.16±0.13 (94.8±1.1%) | 0.34±0.08 (5.2±1.1%) | 1.18±0.03 | 0.78±0.02 |

ability to form synapses was unaffected in GlcAT-P-deficient neurons, but the synapses along dendritic shafts, so-called shaft synapses, were preferentially formed. To investigate the localization of postsynaptic sites in GlcAT-P-deficient neurons, we transfected GFP into hippocampal neurons and immunostained them for PSD-95. Abundant PSD-95 puncta accumulated along dendritic shafts, especially near the bases of the filopodia in GlcAT-P-deficient neurons (Fig. 4C, arrows).

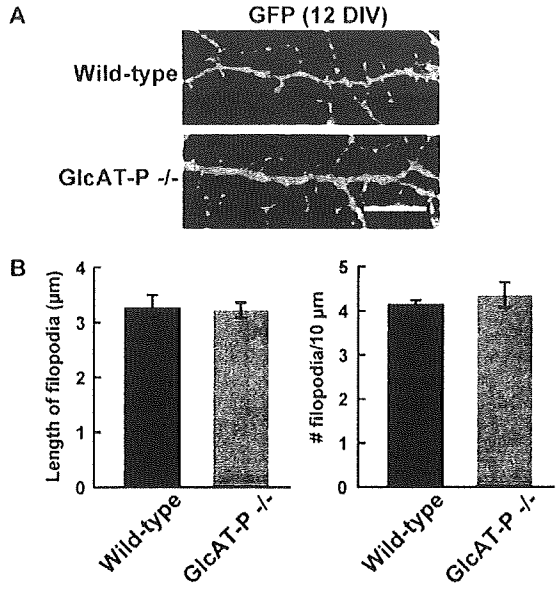


Fig. 3. Normal morphology of filopodia in GlcAT-P −/− neurons. (A) Cultured hippocampal neurons were transfected with GFP at 10 DIV and then immunostained for GFP at 12 DIV. Individual dendrite segments from wild-type and GlcAT-P −/− neurons are presented. Scale bar: 10 μm. (B) Quantification of mean length and filopodia density as in (A) ($n$=3, 3–4 cells and 66–94 filopodia per experiment for wild-type neurons; $n$=3, 3–4 cells and 59–108 filopodia per experiment for GlcAT-P −/− neurons). Histograms show the mean length (left) and the mean density of filopodia (right) of wild-type and GlcAT-P −/− neurons. Error bars indicate SEM. For interpretation of the references to color in this figure legend, the reader is referred to the Web version of this article.

Recently, we identified the AMPA type glutamate receptor subunit GluR2 as a major HNK-1 carrier protein in postsynaptic density (PSD) and demonstrated that the expression of HNK-1 on GluR2 increases its stability on the cell surface (Morita et al., in press). As shown in Fig. 5A, the HNK-1 epitope was expressed on GluR2 in wild-type neurons but not in GlcAT-P-deficient neurons. To examine if HNK-1 alters the subcellular localization of GluR2, hippocampal neurons at 19 DIV were doubly immunostained for GluR2 and MAP-2 (neurite marker protein). The punctate staining of GluR2 was closely localized along MAP-2 staining (dendritic shafts) in GlcAT-P-deficient neurons compared to that in wild-type (Fig. 4D). Next, we performed double immunostaining for GluR2 and postsynaptic maker proteins, (PSD-95, Fig. 4E) and (F-actin, Fig. 4F). The staining of GluR2 was co-localized with PSD-95 or F-actin at postsynaptic sites, but the clusters of these proteins were also localized on dendritic shafts in GlcAT-P-deficient neurons (Fig. 4E, F, arrowheads). To verify these findings, we measured the fluorescence intensities of GluR2 along a line drawn across the dendrites as shown in Fig. 4F. Wild-type neurons showed two separate intensity peaks of GluR2 corresponding to the localization of dendritic spines (Fig. 4G, upper panel). On the other hand, the GluR2 in GlcAT-P-deficient neurons showed a higher intensity in the dendritic shafts and a less specific localization at dendritic spines (Fig. 4G, lower panel). Taken together, loss of HNK-1 did not inhibit functional synapse formation, but excessive numbers of shaft synapses were formed along dendritic shafts, suggesting that the HNK-1 epitope is necessary for the localization of postsynaptic components including GluR2.

### HNK-1 epitope on GluR2 is important for spine morphogenesis

Recent studies have demonstrated that the extracellular N-terminal domain of GluR2 induces spine morphogenesis and that the spine promoting activity of GluR2 is dependent on its interaction with the neural adhesion molecule N-cadherin (Passafaro et al., 2003; Saglietti et al., 2007). Whereas GluR2 were equivalently expressed in wild-type and GlcAT-P-deficient neurons, GluR2 in wild-type neu-

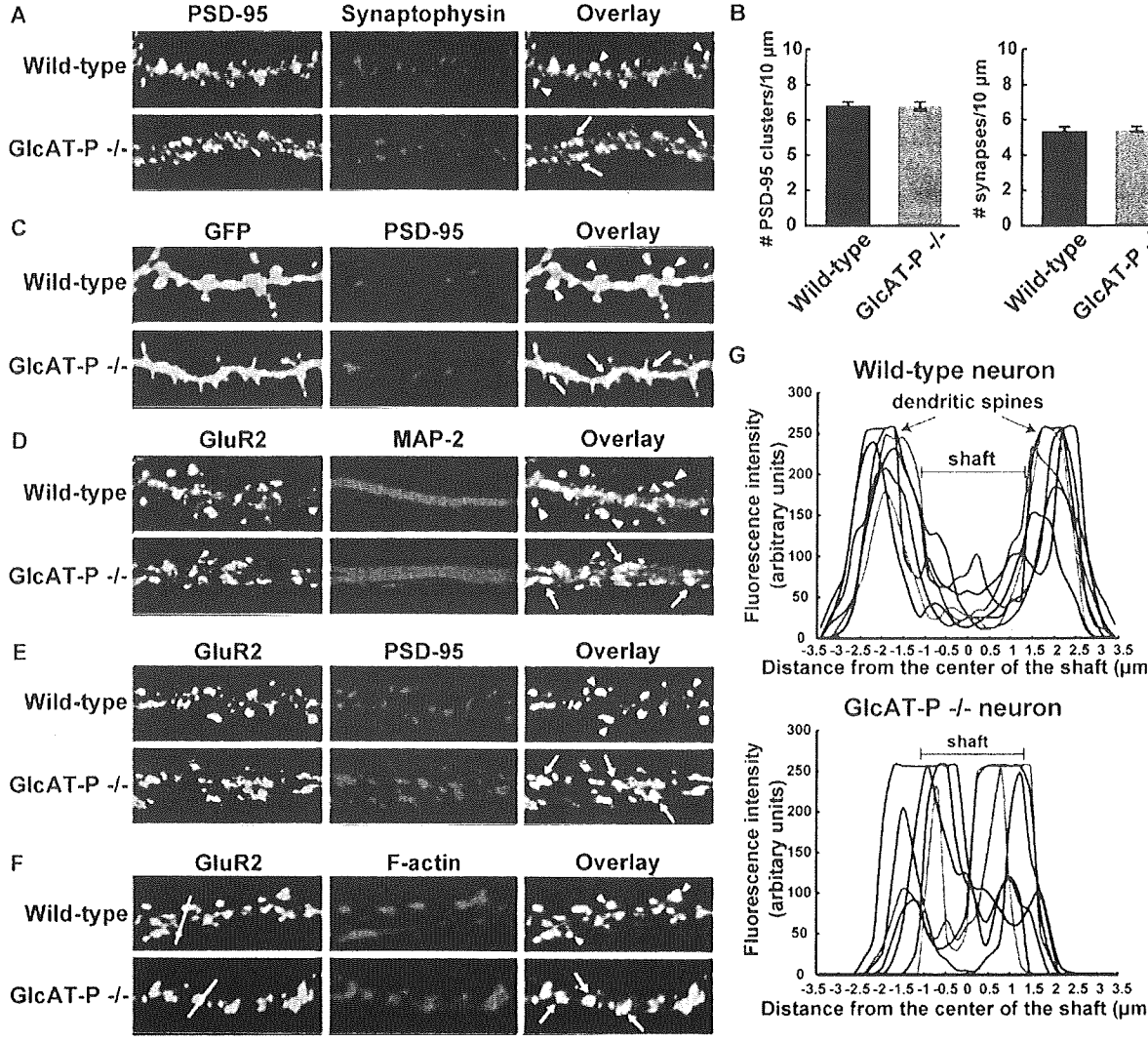


Fig. 4. Effects of HNK-1 on the formation and localization of synapses. (A) Double immunostaining for PSD-95 (green) and synaptophysin (red) in cultured hippocampal neurons at 19 DIV. Arrowheads indicate dendritic synapses in wild-type neurons, and arrows indicate the shaft synapses in GlcAT-P −/− neurons. Note that the PSD-95 puncta on dendritic shafts were also apposed to synaptophysin, indicating the formation of synapses in GlcAT-P −/− neurons. (B) Quantification of the densities of PSD-95 clusters and synapses on dendrites in (A). Histograms show the number of PSD-95 clusters (left) and synapses (right) per 10 μm dendrite. (C) Cultured hippocampal neurons were transfected at 15 DIV with GFP and were then double immunostained for GFP (green) and PSD-95 (red) at 18 DIV. Arrowheads indicate clusters of PSD-95 on spine heads in wild-type neurons, and arrows indicate PSD-95 on dendritic shafts near the bases of filopodia in GlcAT-P −/− neurons. (D) Double immunostaining for GluR2 (green) and MAP-2 (red) in cultured hippocampal neurons at 19 DIV. Arrowheads indicate GluR2 puncta on dendritic spine heads in wild-type neurons, and arrows indicate GluR2 accumulated on dendritic shafts in GlcAT-P −/− neurons. (E) Double immunostaining for GluR2 (green) and PSD-95 (red) in cultured hippocampal neurons at 19 DIV. Arrowheads and arrows indicate the same as in (D). (F) Double immunostaining for GluR2 (green) and F-actin (red) in cultured hippocampal neurons at 19 DIV. Arrowheads and arrows indicate the same as in (D). (G) GluR2 in GlcAT-P −/− neurons showed excessive accumulation on dendritic shafts. For the determination of the localization of GluR2, lines were drawn across the dendrites (yellow lines in (F)), and the fluorescence intensity profiles of GluR2 along the lines were obtained.

rons carries the HNK-1 epitope but that in GlcAT-P-deficient neurons does not (Fig. 5A). We also found that the HNK-1 on GluR2 significantly enhances its interaction with N-cadherin in mouse hippocampus and HEK 293 cells (Morita et al., in press). These results prompted us to examine the possibility that the HNK-1 epitope on GluR2 contributes to spine maturation. So, we co-transfected GFP and GluR2 into wild-type and GlcAT-P-deficient neurons at 13 DIV, before performing analysis at 18 DIV to examine the spine-promoting activity of GluR2. In wild-type neurons, overexpression of GluR2 caused increases in spine length (1.28±0.01 to 1.43±0.03 μm, ** $P<0.01$) and spine width (0.84±0.01 to 1.04±0.01 μm, ** $P<0.01$) (Fig. 5B, C, Table 2), which is consistent with the finding of a previous report (Passafaro et al., 2003; Saglietti et al., 2007). On the other hand, in GlcAT-P-deficient neurons,

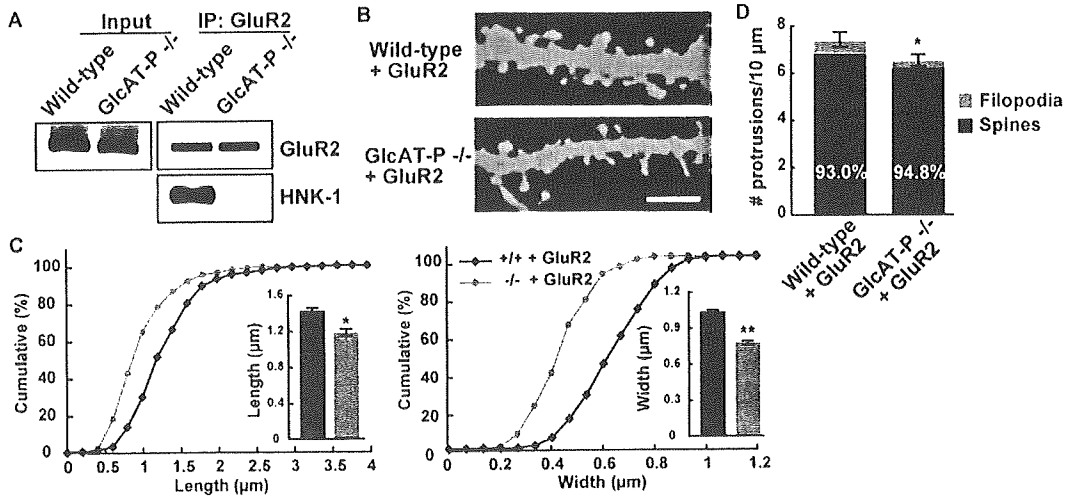


Fig. 5. HNK-1 epitope on GluR2 is crucial for spine morphology. (A) GluR2 was immunoprecipitated from cultured hippocampal neurons. GluR2 in GlcAT-P −/− neurons showed no HNK-1 expression. (B) Representative images of individual dendrite segments of GluR2-overexpressing neurons. Wild-type and GlcAT-P −/− neurons were transfected with GFP and GluR2 at 13 DIV and immunostained for GFP at 18 DIV. Scale bars: 5 μm. (C) Cumulative frequency plots of the spine length and width of dendritic protrusions ($n$=565 for wild-type neurons; $n$=519 for GlcAT-P −/− neurons). $P$<0.01 (Kolmogorov–Smirnov Test). Inset histograms show mean values ($n$=3, 150–232 protrusions per experiment for wild-type neurons; $n$=3, 141–203 protrusions per experiment for GlcAT-P −/− neurons). * $P$<0.05, ** $P$<0.01 (two-tailed $t$-test). (D) The protrusion densities in (C) ($n$=3, 4–5 cells per experiment for wild-type neurons; $n$=3, 5–6 cells per experiment for GlcAT-P −/− neurons). * $P$<0.05 (two-tailed $t$-test). For interpretation of the references to color in this figure legend, the reader is referred to the Web version of this article.

the length of protrusions was decreased (1.71±0.02 to 1.18±0.03 μm, ** $P$<0.01) (Fig. 5B, C, Table 2), due to enhancement of the conversion of filopodia into spines. The spine head width was increased (0.63±0.01 to 0.78±0.02 μm, ** $P$<0.01, Fig. 5B, C, Table 2). Thus, although GluR2 lacking HNK-1 also promotes spine growth, the size (length and width) of the spines in GluR2-overexpressing GlcAT-P-deficient neurons was comparable to that in wild-type neurons but not to that in GluR2-overexpressing wild-type neurons (Table 2). In addition, the spine density was significantly increased by GluR2 overexpression in wild-type neurons (6.23±0.11 to 7.32±0.19, ** $P$<0.01); whereas, it remained unchanged in GlcAT-P-deficient neurons (6.72±0.04 to 6.50±0.21, $P$=0.28). Therefore, the ability of GluR2 to induce spine formation in GlcAT-P-deficient neurons was not as effective as that in wild-type neurons, suggesting that the HNK-1 expressed on GluR2 is important for spine maturation.

## DISCUSSION

The HNK-1 glyco-epitope is widely expressed on some cell adhesion molecules (NCAM, L1, and MAG, etc.) and extracellular matrix molecules (tenascin-R and phosphacan, etc.) in the nervous system (Morita et al., 2008). It has been reported that HNK-1 mediates the interaction of these adhesion molecules, thereby controlling their functions including cell-to-cell adhesion (Kunemund et al., 1988), migration (Bronner-Fraser, 1987), and neurite extension (Martini et al., 1992). In this study, we first demonstrated the involvement of the HNK-1 epitope in normal spine development of hippocampal neurons. Around postnatal 14 days, neural circuits are actively formed, and the HNK-1 epitope shows the highest expression in the mouse brain. At P14, GlcAT-P-deficient CA1 pyramidal neurons showed more immature filopodium-like protrusions than wild-type neurons (Fig. 1A–C). In adult (P70) mice, GlcAT-P-deficient CA1 pyramidal neurons exhibited normal mature mushroom-like spine structures, and there were no significant differences in length and width between wild-type and GlcAT-P-deficient neurons (Fig. 1D–F). The immature filopodium-like protrusions were also observed in GlcAT-P-deficient cultured neurons at 18 DIV (Fig. 2). These morphological impairments were rescued by the expression of GlcAT-P at 15–18 DIV (Fig. 2). However, the overexpression of GlcAT-P had no effect on spine morphology in wild-type neurons (data not shown), indicating that HNK-1 did not promote spines with irregular sizes and shapes. These observations indicate that the HNK-1 epitope specifically influences normal spine maturation in developing brains and that its influence gradually decreases during the course of postnatal development.

As the HNK-1 epitope is almost completely absent from GlcAT-P-deficient mice (Yamamoto et al., 2002), it is very difficult to demonstrate which HNK-1 carrier protein is responsible for normal spine formation. We focused on the HNK-1 on the AMPA-type glutamate receptor subunit GluR2 for the following reasons. First, we identified GluR2 as a major HNK-1 carrier at postsynaptic sites (Morita et al., in press). GluR2 localizes in PSD and is a key molecule in long-term synaptic changes and dendritic spine morphogenesis (Isaac et al., 2007). We also showed that the HNK-1 epitope on GluR2 increased its interaction with N-cadherin and the expression of GluR2 on the neural surface membrane (Morita et al., in press). This interaction

is necessary for the promotion of the enlargement of dendritic spines (Saglietti et al., 2007). Second, in GlcAT-P-deficient neurons, GluR2 and PSD proteins were localized on the shafts of dendrites, and abundant shaft synapses were formed (Fig. 4). It was reported that Rap2, a member of the Rap family of small GTPases, regulated the distribution of GluR2 and AMPA receptor-mediated mEPSC (Fu et al., 2007). Furthermore, the active form of Rap2 caused a reduction in surface GluR2 levels, the loss of dendritic spines, and an increase in filopodium-like protrusions and shaft synapses (Fu et al., 2007). These results are consistent with the phenomena observed in GlcAT-P-deficient neurons (Fig. 4), suggesting that the abnormalities in GlcAT-P-deficient neurons are modulated by reduction of the surface GluR2 level. Third, in a rescue experiment, the transfection of GlcAT-P completely restored spine immaturity in 15 to 18 DIV neurons (Fig. 2). This corresponds well to the time window (15 to 18 DIV) during which GluR2 plays an important role in spine maturation by being translocated from dendritic shafts to forming spine heads (Pickard et al., 2000). Finally, when GluR2 was overexpressed in GlcAT-P-deficient neurons, the maturation of the dendritic spines was not promoted as effectively as in wild-type neurons, indicating that overexpressed GluR2 does not function fully in the absence of the HNK-1 epitope (Fig. 5). These lines of evidence strongly support the notion that GluR2 and HNK-1 modulate spinogenesis in the hippocampus. Although we cannot exclude the possibility that other HNK-1 carrier glycoproteins are involved in spine maturation, HNK-1 on GluR2 must be one of the most critical factors.

We found that excessive numbers of shaft synapses were present in mature GlcAT-P-deficient neurons compared with wild-type neurons (Fig. 4). In general, shaft synapses are considered as precursors of dendritic spine synapses during development and activity-dependent synaptogenesis (Fiala et al., 1998; Ethell and Pasquale, 2005). In young brains, glutamatergic neurons have abundant shaft synapses on their dendrites, and the number of shaft synapses decreases with increase in the number of dendritic spines during brain development (Boyer et al., 1998). On the other hand, recent studies have argued that shaft synapses may have roles other than being the precursor of spine synapses. It was reported that the numbers of shaft and spine synapses are independently regulated by behavioral learning and the induction of synaptic plasticity (Helmeke et al., 2001; Zha et al., 2005; Nikolakopoulou et al., 2006), suggesting that distinct mechanisms are involved in regulation of these two types of synapses. Although it was recently reported that the expression of EphrinB3 and the inhibition of CaMKII promoted shaft synapse formation (Aoto et al., 2007; Zha et al., 2009), the detailed molecular mechanisms behind shaft synapse formation remain unclear. GlcAT-P-deficient mice may provide a good model for understanding the formation of shaft synapses and shaft synapse-related synaptic functions.

As for synaptic plasticity, the HNK-1 epitope carried by tenascin-R has been well characterized. Tenascin-R is abundant in the perineuronal nets surrounding parvalbmin-positive interneurons (Wintergerst et al., 1996; Bruckner et al., 2000). It is proposed that the HNK-1 on tenascin-R reduces GABA release for the perisomatic inhibition of CA1 pyramidal neurons, resulting in the reduction of LTP in CA1 pyramidal neurons (Saghatelyan et al., 2000; Dityatev and Schachner, 2003). Recently, Bukalo et al. demonstrated that the reduction of LTP in tenascin-R-deficient mice is due to increased threshold for induction of LTP, and the peptidomimetic of HNK-1 carbohydrate restored the impaired LTP in tenascin-R-deficient mice, indicating that HNK-1 carried by tenascin-R is important for synaptic plasticity (Bukalo et al., 2007). In this study, we showed that HNK-1 was associated with the morphology of dendritic spines as well as the distribution of AMPA receptors. The impairment of spine maturation in GlcAT-P-deficient mice was gradually reversed during the course of postnatal development *in vivo*. The relationship between impaired spine maturation in developing brains and reduced LTP in adult brains of GlcAT-P-deficient mice remains unclear. It is possible that after the induction of plastic changes at synapses in adult mice, structural differences of spines between wild-type and GlcAT-P-deficient mice becomes evident. While further investigation is necessary to elucidate the overall role of the HNK-1 carbohydrate in synaptic plasticity, our current results suggest that the HNK-1 carried by GluR2 contributes to structural plasticity of dendritic spines.

*Acknowledgments—We would like to thank Drs. A. Ikeda (Kyoto University), T. Seki (Juntendo University), and Y. Yoshihara (RIKEN) for valuable discussions and technical advice. This work was supported in part by a Grant-in-Aid for Scientific Research (B) 21370053 (to S. O) from the Ministry of Education, Culture, Sports, Science and Technology, and by the Mizutani Foundation for Glycoscience (to S. O).*

## REFERENCES

Aoto J, Ting P, Maghsoodi B, Xu N, Henkemeyer M, Chen L (2007) Postsynaptic ephrinB3 promotes shaft glutamatergic synapse formation. J Neurosci 27:7508–7519.

Bakker H, Friedmann I, Oka S, Kawasaki T, Nifant'ev N, Schachner M, Mantei N (1997) Expression cloning of a cDNA encoding a sulfotransferase involved in the biosynthesis of the HNK-1 carbohydrate epitope. J Biol Chem 272:29942–29946.

Boyer C, Schikorski T, Stevens CF (1998) Comparison of hippocampal dendritic spines in culture and in brain. J Neurosci 18:5294–5300.

Bronner-Fraser M (1987) Perturbation of cranial neural crest migration by the HNK-1 antibody. Dev Biol 123:321–331.

Bruckner G, Grosche J, Schmidt S, Hartig W, Margolis RU, Delpech B, Seidenbecher CI, Czaniera R, Schachner M (2000) Postnatal development of perineuronal nets in wild-type mice and in a mutant deficient in tenascin-R. J Comp Neurol 428:616–629.

Bukalo O, Schachner M, Dityatev A (2007) Hippocampal metaplasticity induced by deficiency in the extracellular matrix glycoprotein tenascin-R. J Neurosci 27:6019–6028.

Dailey ME, Smith SJ (1996) The dynamics of dendritic structure in developing hippocampal slices. J Neurosci 16:2983–2994.

Derkach VA, Oh MC, Guire ES, Soderling TR (2007) Regulatory mechanisms of AMPA receptors in synaptic plasticity. Nat Rev Neurosci 8:101–113.

Dityatev A, Schachner M (2003) Extracellular matrix molecules and synaptic plasticity. Nat Rev Neurosci 4:456–468.

Ethell IM, Pasquale EB (2005) Molecular mechanisms of dendritic spine development and remodeling. Prog Neurobiol 75:161–205.
Fiala JC, Feinberg M, Popov V, Harris KM (1998) Synaptogenesis via dendritic filopodia in developing hippocampal area CA1. J Neurosci 18:8900–8911.
Fu Z, Lee SH, Simonetta A, Hansen J, Sheng M, Pak DT (2007) Differential roles of Rap1 and Rap2 small GTPases in neurite retraction and synapse elimination in hippocampal spiny neurons. J Neurochem 100:118–131.
Helmeke C, Ovtscharoff W Jr, Poeggel G, Braun K (2001) Juvenile emotional experience alters synaptic inputs on pyramidal neurons in the anterior cingulate cortex. Cereb Cortex 11:717–727.
Hering H, Sheng M (2001) Dendritic spines: structure, dynamics and regulation. Nat Rev Neurosci 2:880–888.
Isaac JT, Ashby M, McBain CJ (2007) The role of the GluR2 subunit in AMPA receptor function and synaptic plasticity. Neuron 54:859–871.
Kleene R, Schachner M (2004) Glycans and neural cell interactions. Nat Rev Neurosci 5:195–208.
Kunemund V, Jungalwala FB, Fischer G, Chou DK, Keilhauer G, Schachner M (1988) The L2/HNK-1 carbohydrate of neural cell adhesion molecules is involved in cell interactions. J Cell Biol 106:213–223.
Liedtke S, Geyer H, Wuhrer M, Geyer R, Frank G, Gerardy-Schahn R, Zahringer U, Schachner M (2001) Characterization of N-glycans from mouse brain neural cell adhesion molecule. Glycobiology 11:373–384.
Martini R, Xin Y, Schmitz B, Schachner M (1992) The L2/HNK-1 carbohydrate epitope is involved in the preferential outgrowth of motor neurons on ventral roots and motor nerves. Eur J Neurosci 4:628–639.
Matsuno H, Okabe S, Mishina M, Yanagida T, Mori K, Yoshihara Y (2006) Telencephalin slows spine maturation. J Neurosci 26: 1776–1786.
Morita I, Kakuda S, Takeuchi Y, Itoh S, Kawasaki N, Kizuka Y, Kawasaki T, Oka S (in press) HNK-1 glyco-epitope regulates the stability of the glutamate receptor subunit GluR2 on the neuronal cell surface. J Biol Chem, in press.
Morita I, Kizuka Y, Kakuda S, Oka S (2008) Expression and function of the HNK-1 carbohydrate. J Biochem 143:719–724.
Nikolakopoulou AM, Davies HA, Stewart MG (2006) Passive avoidance training decreases synapse density in the hippocampus of the domestic chick. Eur J Neurosci 23:1054–1062.
Ohtsubo K, Marth JD (2006) Glycosylation in cellular mechanisms of health and disease. Cell 126:855–867.
Passafaro M, Nakagawa T, Sala C, Sheng M (2003) Induction of dendritic spines by an extracellular domain of AMPA receptor subunit GluR2. Nature 424:677–681.
Pasternack A, Coleman SK, Fethiere J, Madden DR, LeCaer JP, Rossier J, Pasternack M, Keinanen K (2003) Characterization of the functional role of the N-glycans in the AMPA receptor ligand-binding domain. J Neurochem 84:1184–1192.
Pickard L, Noel J, Henley JM, Collingridge GL, Molnar E (2000) Developmental changes in synaptic AMPA and NMDA receptor distribution and AMPA receptor subunit composition in living hippocampal neurons. J Neurosci 20:7922–7931.
Saghatelyan AK, Gorissen S, Albert M, Hertlein B, Schachner M, Dityatev A (2000) The extracellular matrix molecule tenascin-R and its HNK-1 carbohydrate modulate perisomatic inhibition and long-term potentiation in the CA1 region of the hippocampus. Eur J Neurosci 12:3331–3342.
Saglietti L, Dequidt C, Kamieniarz K, Rousset MC, Valnegri P, Thoumine O, Beretta F, Fagni L, Choquet D, Sala C, Sheng M, Passafaro M (2007) Extracellular interactions between GluR2 and N-cadherin in spine regulation. Neuron 54:461–477.
Sakimura K, Bujo H, Kushiya E, Araki K, Yamazaki M, Yamazaki M, Meguro H, Warashina A, Numa S, Mishina M (1990) Functional expression from cloned cDNAs of glutamate receptor species responsive to kainate and quisqualate. FEBS Lett 272:73–80.
Segal M (2005) Dendritic spines and long-term plasticity. Nat Rev Neurosci 6:277–284.
Seiki T, Oka S, Terayama K, Imiya K, Kawasaki T (1999) Molecular cloning and expression of a second glucuronyltransferase involved in the biosynthesis of the HNK-1 carbohydrate epitope. Biochem Biophys Res Commun 255:182–187.
Senn C, Kutsche M, Saghatelyan A, Bosl MR, Lohler J, Bartsch U, Morellini F, Schachner M (2002) Mice deficient for the HNK-1 sulfotransferase show alterations in synaptic efficacy and spatial learning and memory. Mol Cell Neurosci 20:712–729.
Terayama K, Oka S, Seiki T, Miki Y, Nakamura A, Kozutsumi Y, Takio K, Kawasaki T (1997) Cloning and functional expression of a novel glucuronyltransferase involved in the biosynthesis of the carbohydrate epitope HNK-1. Proc Natl Acad Sci U S A 94:6093–6098.
Wintergerst ES, Vogt Weisenhorn DM, Rathjen FG, Riederer BM, Lambert S, Celio MR (1996) Temporal and spatial appearance of the membrane cytoskeleton and perineuronal nets in the rat neocortex. Neurosci Lett 209:173–176.
Yamamoto S, Oka S, Inoue M, Shimuta M, Manabe T, Takahashi H, Miyamoto M, Asano M, Sakagami J, Sudo K, Iwakura Y, Ono K, Kawasaki T (2002) Mice deficient in nervous system-specific carbohydrate epitope HNK-1 exhibit impaired synaptic plasticity and spatial learning. J Biol Chem 277:27227–27231.
Yoshihara T, Sugihara K, Kizuka Y, Oka S, Asano M (2009) Learning/memory impairment and reduced expression of the HNK-1 carbohydrate in beta 4-galactosyltransferase-II-deficient mice. J Biol Chem 284:12550–12561.
Zha XM, Dailey ME, Green SH (2009) Role of $Ca2^+$/calmodulin-dependent protein kinase II in dendritic spine remodeling during epileptiform activity in vitro. J Neurosci Res 87:1969–1979.
Zha XM, Green SH, Dailey ME (2005) Regulation of hippocampal synapse remodeling by epileptiform activity. Mol Cell Neurosci 29:494–506.
Zhang H, Macara IG (2006) The polarity protein PAR-3 and TIAM1 cooperate in dendritic spine morphogenesis. Nat Cell Biol 8: 227–237.
Ziv NE, Smith SJ (1996) Evidence for a role of dendritic filopodia in synaptogenesis and spine formation. Neuron 17:91–102.

## APPENDIX

### Supplementary data

Supplementary data associated with this article can be found, in the online version, at doi:10.1016/j.neuroscience.2009.09.065.

*(Accepted 24 September 2009)*
*(Available online 29 September 2009)*

THE JOURNAL OF BIOLOGICAL CHEMISTRY VOL. 284, NO. 44, pp. 30209–30217, October 30, 2009


# HNK-1 Glyco-epitope Regulates the Stability of the Glutamate Receptor Subunit GluR2 on the Neuronal Cell Surface*[S]

Received for publication, May 21, 2009, and in revised form, August 9, 2009 Published, JBC Papers in Press, September 3, 2009, DOI 10.1074/jbc.M109.024208

Ippei Morita[‡1], Shinako Kakuda[§1], Yusuke Takeuchi[§], Satsuki Itoh[¶], Nana Kawasaki[¶], Yasuhiko Kizuka[‡], Toshisuke Kawasaki[‖], and Shogo Oka[§2]

*From the [‡]Department of Biological Chemistry, Graduate School of Pharmaceutical Sciences, and [§]Department of Biological Chemistry, Human Health Sciences, Graduate School of Medicine, Kyoto University, Kyoto 606-8507, the [¶]Division of Biological Chemistry and Biologicals, National Institute of Health Sciences, Tokyo 158-8501, and the [‖]Research Center for Glycobiotechnology, Ritsumeikan University, Shiga 525-8577, Japan*

**HNK-1 (human natural killer-1) glyco-epitope, a sulfated glucuronic acid attached to *N*-acetyllactosamine on the nonreducing termini of glycans, is highly expressed in the nervous system. Our previous report showed that mice lacking a glucuronyltransferase (GlcAT-P), a key enzyme for biosynthesis of the HNK-1 epitope, showed reduced long term potentiation at hippocampal CA1 synapses. In this study, we identified an α-amino-3-hydroxy-5-methylisoxazole propionate (AMPA)-type glutamate receptor subunit, GluR2, which directly contributes to excitatory synaptic transmission and synaptic plasticity, as a novel HNK-1 carrier molecule. We demonstrated that the HNK-1 epitope is specifically expressed on the *N*-linked glycan(s) on GluR2 among the glutamate receptors tested, and the glycan structure, including HNK-1 on GluR2, was determined using liquid chromatography-tandem mass spectrometry. As for the function of HNK-1 on GluR2, we found that the GluR2 not carrying HNK-1 was dramatically endocytosed and expressed less on the cell surface compared with GluR2 carrying HNK-1 in both cultured hippocampal neurons and heterologous cells. These results suggest that HNK-1 stabilizes GluR2 on neuronal surface membranes and regulates the number of surface AMPA receptors. Moreover, we showed that the expression of the HNK-1 epitope enhanced the interaction between GluR2 and N-cadherin, which has important roles in AMPA receptor trafficking. Our findings suggest that the HNK-1 epitope on GluR2 regulates cell surface stability of GluR2 by modulating the interaction with N-cadherin.**

HNK-1 glyco-epitope ($HSO_3$-3GlcAβ1–3Galβ1–4GlcNAc) is characteristically expressed on some cell adhesion molecules (NCAM, L1, and MAG, etc.) and extracellular matrix molecules (tenascin-R and phosphacan, etc.) in the nervous system (1). It has been reported that HNK-1 mediates the interaction of these adhesion molecules, thereby controlling their functions, including cell-to-cell adhesion (2), migration (3), and neurite extension (4). The unique structural feature of the HNK-1 epitope is the sulfated glucuronic acid, because sialic acids are usually attached to the terminal galactose residue of the inner *N*-acetyllactosamine structure, (Galβ1–4GlcNAc) on various glycoproteins. HNK-1 is sequentially biosynthesized by one of two glucuronyltransferases (GlcAT-P or GlcAT-S)[3] (5, 6) and a sulfotransferase (HNK-1ST) (7). These enzymes are thought to localize and function in the Golgi apparatus, especially the trans-Golgi to trans-Golgi network, like most sialyltransferases and galactosyltransferases (8).

We previously demonstrated that mice deficient in GlcAT-P showed an almost complete loss of HNK-1 expression in the brain and exhibited reduced LTP in hippocampal CA1 synapses (9). Similarly, HNK-1ST-deficient mice also exhibited a reduction of LTP, and several other studies also revealed that HNK-1 is associated with neural plasticity (10–12). A recent study showed that β4-galactosyltransferase-2 synthesizes the glycan backbone structure of HNK-1, Galβ1–4GlcNAc. The mice lacking β4-galactosyltransferase-2 showed decreased HNK-1 expression in their brains and also exhibited impaired learning and memory (13). Overall, these studies suggest that HNK-1 plays unique functional roles in some types of neuronal plasticity, but the molecular mechanisms of HNK-1 remain unclear.

AMPA-type glutamate receptors mediate most of the fast excitatory synaptic transmissions in the mammalian brain and control synaptic strength. The regulated trafficking of AMPA receptors to the postsynaptic membrane is thought to be a major mechanism contributing to long lasting changes in synaptic strength, including LTP and long term depression (14, 15). AMPA receptors are mainly heterotetrameric channels assembled from the subunits GluR1 to GluR4, and all subunits have 4–6 potential *N*-glycosylation sites in their extracellular domains (16). Few studies have focused on the function of

* This work was supported in part by Grant-in-aid for Scientific Research (B) 21370053 (to S. O.) from the Ministry of Education, Culture, Sports, Science and Technology and by the Mizutani Foundation for Glycoscience (to S. O.).

[S] The on-line version of this article (available at http://www.jbc.org) contains supplemental Figs. S1 and S2.

[1] Both authors contributed equally to this work.

[2] To whom correspondence should be addressed: Kawahara-cho 53, Shogoin, Sakyo-ku, Kyoto 606-8507, Japan. Tel./Fax: 81-75-751-3959; E-mail: shogo@hs.med.kyoto-u.ac.jp.

[3] The abbreviations used are: GlcAT, glucuronyltransferase; AMPA, α-amino-3-hydroxy-5-methylisoxazole propionate; FT-ICR MS, Fourier transform-ion cyclotron resonance mass spectrometer; LC/MS/MS, liquid chromatography-tandem mass spectrometry; LTP, long term potentiation; PSD, postsynaptic density; CHO, Chinese hamster ovary; DTSSP, 3,3′-dithiobis(sulfosuccinimidyl propionate); P, postnatal day; ST, sulfotransferase.

*N*-glycosylation in AMPA receptors. Some investigations showed that AMPA receptor subunits expressed at both the cell surface and synaptic sites possess the mature glycosylated form (17, 18), but it is generally accepted that *N*-glycosylation is not essential for their channel function or ligand binding (19, 20).

In this study, we searched for a candidate molecule(s) responsible for the defects in synaptic plasticity seen in GlcAT-P-deficient mice. We found that the HNK-1 epitope is mainly expressed on a specific molecule in the hippocampal postsynaptic density (PSD) fraction. We focused on the molecule and identified a subunit of AMPA-type glutamate receptors, GluR2, as a novel HNK-1 carrier protein. Furthermore, we showed that the loss of HNK-1 epitope on GluR2 greatly increases both constitutive and regulated endocytosis of GluR2, resulting in a decrease in the amount of surface GluR2 in cultured hippocampal neurons and CHO cells. This is the first report demonstrating that the *N*-glycan on GluR2 regulates its protein function, and our results suggest that HNK-1 epitope on GluR2 is an important factor for synaptic plasticity.

## EXPERIMENTAL PROCEDURES

*Expression Plasmids*—The following mammalian expression plasmids have been described. The 3.2-kb XhoI-XbaI GluR2 fragment derived from pKC24 (pBluescript)-GluR2, which was donated by Dr. M. Mishina (Tokyo University) (21), was cloned into pcDNA3.1/myc-HisB (Invitrogen) to yield the plasmid pcDNA3.1-GluR2. The pIRES-GlcAT-P-HNK-1ST and pEF-BOS-GlcAT-P plasmids were described previously (5, 22). The pcDNA3.1-N-cadherin was a generous gift from Dr. A. Kinoshita (Kyoto University) (23).

*Biochemical Subcellular Fractionation*—Biochemical subcellular fractionation was performed according to the method of a previous report (24) with minor modifications. The hippocampi of C57 BL/6 mice were homogenized with 15 strokes at 800 rpm in 9 volumes of ice-cold homogenizing buffer (10 mM Tris-HCl (pH 7.4), 0.32 M sucrose, 1 mM EDTA, and protease inhibitor mixture (Nacalai Tesque)), and the homogenate was centrifuged at 1,000 × *g* for 20 min to remove nuclei and large debris. The supernatant fluid (S1, postnuclear fraction) was centrifuged at 10,000 × *g* for 20 min to pellet a crude synaptosome fraction (P2). The supernatant above the P2 fraction was centrifuged at 125,000 × *g* for 1 h, and the pellet was designated as the light membrane fraction (P3). The P2 fraction was lysed hypo-osmotically and centrifuged at 25,000 × *g* for 30 min to obtain the synaptosomal membrane fraction (LP1). The LP1 fraction was then suspended in 0.5% Triton X-100 in homogenizing buffer for 15 min and centrifuged at 125,000 × *g* for 1 h to obtain the PSD fraction. All biochemical experiments were carried out on ice or at 4 °C. The protein concentration of each fraction was measured with DC protein assay kit (Bio-Rad).

*Purification and Identification of Glycoproteins Bearing HNK-1 Epitope*—HNK-1 carrier glycoproteins from the P2 fraction of the hippocampi were partially purified with HNK-1 antibody-conjugated beads. The purified proteins were isolated by SDS-PAGE and stained with Coomassie Brilliant Blue. The ~100-kDa protein band was digested with trypsin, and the peptide fragments were identified by LC/MS/MS as reported previously (25). Proteins were identified by searching Swiss Protein Database (mouse) using the Mascot (Matrixscience) and TurboSequest search engines (Thermo Fisher Scientific).

*SDS-PAGE, Immunoblot, and Immunoprecipitation Analysis*—Proteins were separated by SDS-PAGE with the buffer system of Laemmli (26) and then transferred to a nitrocellulose membrane. After blocking with 5% nonfat dried milk in phosphate-buffered saline containing 0.1% Tween 20, the membrane was incubated with primary antibodies. Horseradish peroxidase-conjugated secondary antibodies and ECL (Pierce) were used for protein detection. For immunoprecipitation under denaturing conditions, the PSD fraction was solubilized with 1 volume of 10 mM Tris-HCl (pH 7.4) buffer containing 1% SDS and boiled for 5 min, and then 5 volumes of immunoprecipitation buffer (20 mM Tris-HCl (pH 7.4), 2% Triton X-100, and 300 mM NaCl) and 4 volumes of $H_2O$ were added to the sample. For immunoprecipitation under native conditions, HEK 293 cells were lysed with extraction buffer (20 mM Tris-HCl (pH 7.4), 1% Triton X-100, 0.5% deoxycholate, 150 mM NaCl, 1 mM EDTA, and protease inhibitor mixture). Primary antibodies were used at 4 μg/ml, and 20 μl of protein G-Sepharose 4 Fast Flow (GE Healthcare) were added to precipitate the immunocomplexes for 2 h at 4 °C. The antibodies used in the immunoprecipitation and immunoblot analyses are listed as follows: HNK-1 monoclonal antibody (a hybridoma cell line was purchased from the American Type Culture Collection); anti-actin N terminus (Sigma); anti-PSD-95 (Chemicon); anti-GluR1 N terminus and anti-GluR2 N terminus (Zymed Laboratories Inc.); GluR2/3 (Upstate); anti-NR1 (Upstate); anti-NR2A (Upstate); anti-synaptophysin (FabGennix); and anti-N-cadherin (BD Biosciences).

*N-Glycosidase F Digestion*—The immunoprecipitates formed with the anti-GluR1 and anti-GluR2 antibodies were denatured with 20 mM sodium phosphate buffer (pH 7.2) containing 0.5% SDS, 1% 2-mercaptoethanol, and 4 mM EDTA. To reduce the concentration of SDS, we diluted the samples with 4 volumes of 20 mM sodium phosphate buffer (pH 7.2) containing 0.5% Nonidet P-40. Two units of *N*-glycosidase F (Roche Applied Science) were added to the solution, and the solution was incubated for 16 h at 37 °C.

*Purification of GluR2*—Anti-GluR2 antibody was raised from a rabbit immunized with a 20-mer peptide (QNFATYKEGYNVYGIESVKI) corresponding to the C terminus of mouse GluR2 and purified with an antigen peptide affinity column. The purified anti-GluR2 antibody (3 mg) was coupled to 1.5 ml of CNBr-activated Sepharose 4B (GE healthcare), and the resin was packed into a column. The P2 fractions from 4-week-old mouse hippocampi were extracted with extraction buffer containing 1% *n*-dodecyl-β-D-maltopyranoside. The extracted material was slowly applied to the anti-GluR2 antibody column. After washing the column with Tris-buffered saline containing 0.1% *n*-dodecyl-β-D-maltopyranoside, GluR2 proteins bound to the resin were eluted with the elution buffer (50 mM diethylamine (pH 11.0), 150 mM NaCl, and 0.1% *n*-dodecyl-β-D-maltopyranoside). This eluate was immediately neutralized with 0.5 M $NaH_2PO_4$ (pH 4.5). The purified GluR2 was concentrated and subjected to SDS-PAGE.

*LC/MS/MS of N-Linked Oligosaccharides*—The bands of purified GluR2 (~100 kDa) were excised and cut into pieces. The gel pieces were destained and dehydrated with 50% acetonitrile. The protein in the gel was reduced and carboxymethylated by incubation with dithiothreitol and sodium monoiodoacetate (27). *N*-Glycans were extracted from the gel pieces as reported (28) and reduced with $NaBH_4$. The borohydride-reduced glycans were desalted with Envi-carb (Supelco). LC/MS/MS was carried out on a quadrupole linear ion trap/Fourier transform-ion cyclotron resonance mass spectrometer (FT-ICR MS) (Thermo Electron Corp) connected to a NanoLC system (Michrom BioResource, Inc.). The eluents were 5 mM ammonium acetate (pH 9.6), 2% $CH_3CN$ (pump A), and 5 mM ammonium acetate (pH 9.6), 80% $CH_3CN$ (pump B). The borohydride-reduced *N*-linked oligosaccharides were separated on a Hypercarb (0.1 × 150 mm, 5 μm; Thermo Electron Corp.) with a linear gradient of 5–20% of pump B (0–45 min), 20–50% of pump B (45–90 min), 50–70% of pump B (90–90.1 min), and 70% of pump B (90.1–130 min). A full MS scan (*m/z* 700–2000) by FT-ICR MS followed by data-dependent MS/MS for the most abundant ion was performed in the positive ion mode.

*Cell Culture and Transfection*—Primary hippocampal cultures were prepared from postnatal day 0 mouse brains. Hippocampi were trypsinized for 10 min at 37 °C. Dissociated neurons were plated on BD Biocoat Poly-D-lysine Cellware 4-well culture slide (BD Biosciences) at $1.0 \times 10^5$ cells per well coated with 2 μg/ml laminin in Neurobasal medium (Invitrogen) supplemented with 2% B-27 (Invitrogen) and 500 μM L-glutamine. Every 7 days, the cultures were fed by replacing half of the medium with feeding medium. HEK 293 cells were cultured in Dulbecco's modified Eagle's medium with 10% fetal calf serum, and CHO cells were maintained in minimum Eagle's α-medium supplemented with 10% fetal calf serum. These cells were transfected using FuGENE 6 transfection reagent (Roche Applied Science).

*Immunofluorescence-based Internalization Assays*—Live hippocampal neurons were prelabeled with 10 μg/ml anti-GluR2 N terminus antibody for 15 min at 37 °C. After washing out the antibody, the neurons were incubated with or without 100 μM AMPA treatment (in the presence of 50 μM D-2-amino-5-phosphonopentanoic acid) for 20 min at 37 °C to allow endocytosis of GluR2. To stain GluR2 remaining on the cell surface, neurons were fixed in 4% paraformaldehyde, 4% sucrose for 10 min at room temperature and incubated with Alexa 488-conjugated secondary antibody (Molecular Probes) for 1 h at room temperature. The neurons were fixed with methanol at −20 °C, and Alexa 546-conjugated secondary antibody (Molecular Probes) was used for internalized GluR2 staining. Internalized and surface GluR2 fluorescence intensity was quantified using FluoView (Olympus) imaging system.

*Cell Surface Protein Biotinylation Assay*—Hippocampal cultured neurons and CHO cells were reacted with 1 mg/ml EZ-Link Sulfo-NHS-SS-biotin (Pierce) in phosphate-buffered saline for 30 min at 4 °C. Before surface biotinylation, neurons were incubated with or without 100 μM AMPA treatment for 20 min at 37 °C. These cells were lysed with extraction buffer, and cell surface-biotinylated proteins were pulled down with immobilized streptavidin (Pierce) and immunoblotted with anti-GluR2 antibody.

*Cross-linking Experiment*—Hippocampal P2 fractions and transfected HEK 293 cells were cross-linked with 2 mM 3,3′-dithiobis(sulfosuccinimidyl propionate) (DTSSP) (Pierce) in phosphate-buffered saline at room temperature for 30 min, and the reaction was quenched by the addition of 50 mM Tris-HCl (pH 7.4). The cross-linked P2 fractions were solubilized with extraction buffer and centrifuged at 125,000 × *g* for 1 h to separate into two distinct fractions (1% Triton X-100-soluble and -insoluble fractions). The Triton X-100-insoluble fraction was solubilized with 10 mM Tris-HCl (pH 7.4) buffer containing 1% SDS. Both insoluble and soluble fractions were subjected to immunoprecipitation analysis.

*Quantification and Statistical Analysis of Immunoprecipitation Experiment*—For the immunoblot analysis, a luminoimage analyzer LAS-3000 (Fuji Film) was used for the detection of protein bands. Densitometry of these bands was performed using image analysis software ImageGauge (Fuji Film). Calibration curves of protein bands for GluR2 and N-cadherin showed good linearity ($r^2$ = 0.97072 (N-cadherin) and 0.95566 (GluR2)). To quantify the strength of interaction between GluR2 and N-cadherin, the intensity of co-immunoprecipitated N-cadherin or GluR2 was normalized by immunoprecipitated GluR2 or N-cadherin, respectively. Results are shown as percent of value relative to the wild-type or control cells. The statistical analyses performed are listed in the individual figure legends, and values are expressed as the means ± S.E.

## RESULTS

*Expression of HNK-1 Glyco-epitope in the Mouse Hippocampus*—To search for a novel HNK-1 carrier protein(s) responsible for synaptic plasticity, we first examined the expression of HNK-1 glyco-epitope in P2 (crude synaptosome) fractions obtained from mouse hippocampi at several developmental stages (Fig. 1*A*). The expression of HNK-1 was barely detected at embryonic day 16. After birth, it reached a peak at postnatal day 14 (P14), which coincided with the major postnatal synaptogenic period, and gradually decreased in adulthood. The expression of HNK-1 epitope was almost abolished in GlcAT-P-deficient mice (Fig. 1*A*), indicating that the biosynthesis of HNK-1 in brains is mainly regulated by a brain-specific glucuronyltransferase (GlcAT-P). Next, we performed biochemical fractionation of mouse hippocampi and examined the subcellular distribution of the HNK-1 epitope by immunoblot analysis. HNK-1 carrier proteins were detected in a wide range of molecular mass, from 100 to 250 kDa or higher (Fig. 1*B*, *upper panel*), and an ~100-kDa HNK-1-positive band was highly enriched in the P2 and PSD fractions, showing a similar distribution profile to the postsynaptic marker PSD-95 (Fig. 1*B*, *lower panel*). We also examined the subcellular localization of the HNK-1 epitope in cultured hippocampal neurons at 19 days *in vitro*. The immunoreactivity against the HNK-1 antibody was diffusely distributed on dendritic shafts and spine heads (supplemental Fig. 1). **The punctate staining pattern for HNK-1 on the spines was co-localized with PSD-95 and apposed to the presynaptic marker synaptophysin. These results indicated the presence of HNK-1 carrier protein(s) at postsynaptic sites, and**

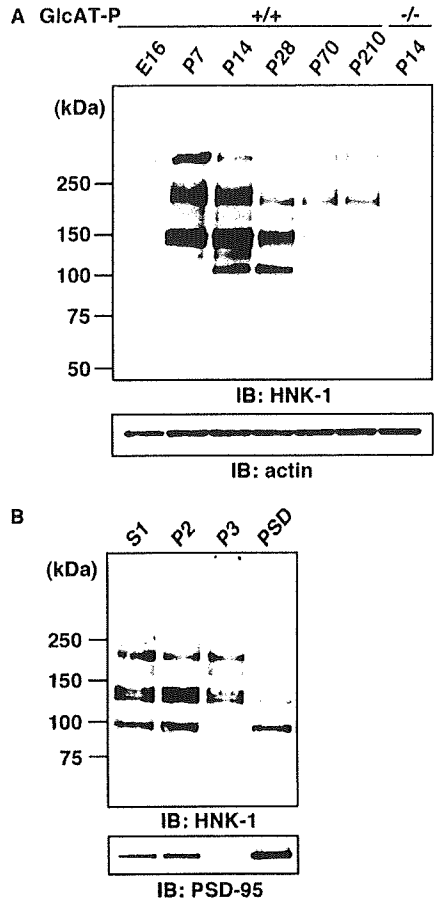


FIGURE 1. **HNK-1 is expressed in the PSD fraction from mouse hippocampi.** *A*, developmental expression of HNK-1 glyco-epitope in mouse hippocampi. Hippocampal P2 fractions (5 $\mu$g of proteins) obtained at the indicated developmental stages (*E16*, embryonic day 16; *P7* to *P210*, postnatal day 7–210) were immunoblotted (*IB*) with HNK-1 monoclonal antibody. Note that the expression of HNK-1 completely disappeared at P14 in the GlcAT-P$^{-/-}$ mice (*right lane*). *B*, biochemical fractionation of HNK-1 carrier proteins and PSD-95 in hippocampi. (*S1*, postnuclear supernatant; *P2*, crude synaptosome; *P3*, light membrane). Five micrograms of proteins obtained from different fractions were immunoblotted for HNK-1 and PSD-95.

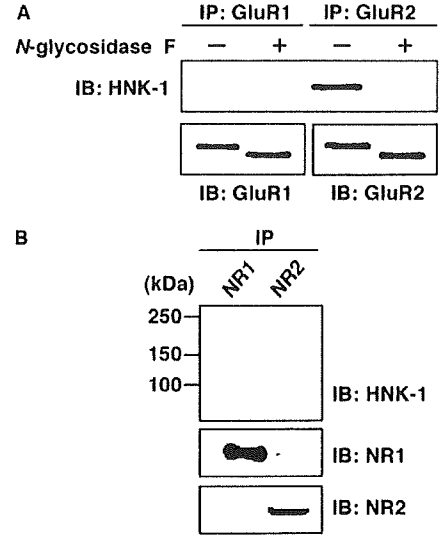


FIGURE 2. **Immunoprecipitation analysis of the PSD fractions from mouse hippocampi.** *A*, GluR1 and GluR2 were immunoprecipitated (*IP*) with GluR1- and GluR2-specific antibodies under SDS-denaturing conditions, respectively. The immunoprecipitates were treated with (+) or without (−) *N*-glycosidase F and then immunoblotted (*IB*) for HNK-1 (*upper panel*) and GluR1 or GluR2 (*lower panel*). *B*, NR1 and NR2 were immunoprecipitated and immunoblotted with HNK-1 antibody (*upper panel*), NR1 (*middle panel*), and NR2 (*lower panel*).

we focused on the specific HNK-1 carrier molecule enriched at postsynaptic sites to examine the role of HNK-1 in synaptic plasticity.

*HNK-1 Glyco-epitope Is Expressed on the AMPA-type Glutamate Receptor Subunit GluR2*—To identify the ~100-kDa candidate glycoprotein, we purified HNK-1 carrier proteins from the P2 fractions of mouse hippocampi using HNK-1 antibody-conjugated beads. The purified proteins were isolated by SDS-PAGE and stained with Coomassie Brilliant Blue. A piece of polyacrylamide gel containing the ~100-kDa glycoprotein was excised and digested with trypsin. Using LC/MS/MS, we identified the novel HNK-1 carrier molecule as GluR2, which is an AMPA-type glutamate receptor subunit (supplemental Fig. 2). To further confirm these results, we immunoprecipitated GluR1 and GluR2 by subunit-specific antibodies from the PSD fractions of hippocampi under denaturing conditions and then immunoblotted them with HNK-1 antibody (Fig. 2*A*). HNK-1 epitope was specifically detected on GluR2 but not on GluR1. Furthermore, the HNK-1 epitope on GluR2 was completely removed by *N*-glycosidase F treatment, indicating that it is attached to the nonreducing terminus of *N*-glycan(s) on GluR2. We also examined the expression of HNK-1 on *N*-methyl-D-aspartic acid (NMDA) receptor (composed of NR1 and NR2 subunits), which is another ionotropic glutamate receptor (Fig. 2*B*). Neither NR1 nor NR2 carried the HNK-1 epitope. These results suggest that the HNK-1 epitope is specifically expressed on GluR2 and may regulate the function of GluR2.

*LC/MS/MS of N-Linked Oligosaccharides on GluR2*—To determine the glycan structure, including HNK-1 glyco-epitope on GluR2, GluR2 was immunopurified from P2 fractions and separated by SDS-PAGE (Fig. 3*A*). The GluR2 band (~100 kDa) was excised and treated with *N*-glycosidase F. The extracted *N*-linked oligosaccharides were reduced with $NaBH_4$ and subjected to LC/MS/MS. Fig. 3*B* shows the base peak chromatograms obtained by a full MS scan (*m/z* 700–2000) by FT-ICR MS. The major molecular ions detected by a full MS scan were subjected to data-dependent collision-induced dissociation-tandem mass spectrometry automatically. From all the MS/MS spectra, only those of oligosaccharides carrying HNK-1 or nonsulfated HNK-1 motifs were sorted out using HNK-1 diagnostic ion, GlcA-Gal-GlcNAc$^+$ (*m/z* 542) (Fig. 3*B*, *lower panel*). The carbohydrate structure of the HNK-1 and nonsulfated HNK-1 oligosaccharides (peaks 1–6) was deduced from the *m/z* values of precursor ions detected by FT-ICR MS and product ions obtained by MS/MS (Fig. 3*C*). As a typical MS/MS spectrum, the product ion spectrum of peak 3 is shown in Fig. 3*D*. Peak 3 was assigned to a bisected biantennary *N*-glycan carrying the HNK-1 motif based on the product ions, such as GlcA-Gal-GlcNAc$^+$ (*m/z* 542), $SO_3$-GlcA-Gal-GlcNAc$^+$ (*m/z* 622), and [M-$SO_3$-GlcA-Gal-GlcNAc + H]$^+$ (*m/z* 1319). Together with the immunoprecipitation experiment shown in

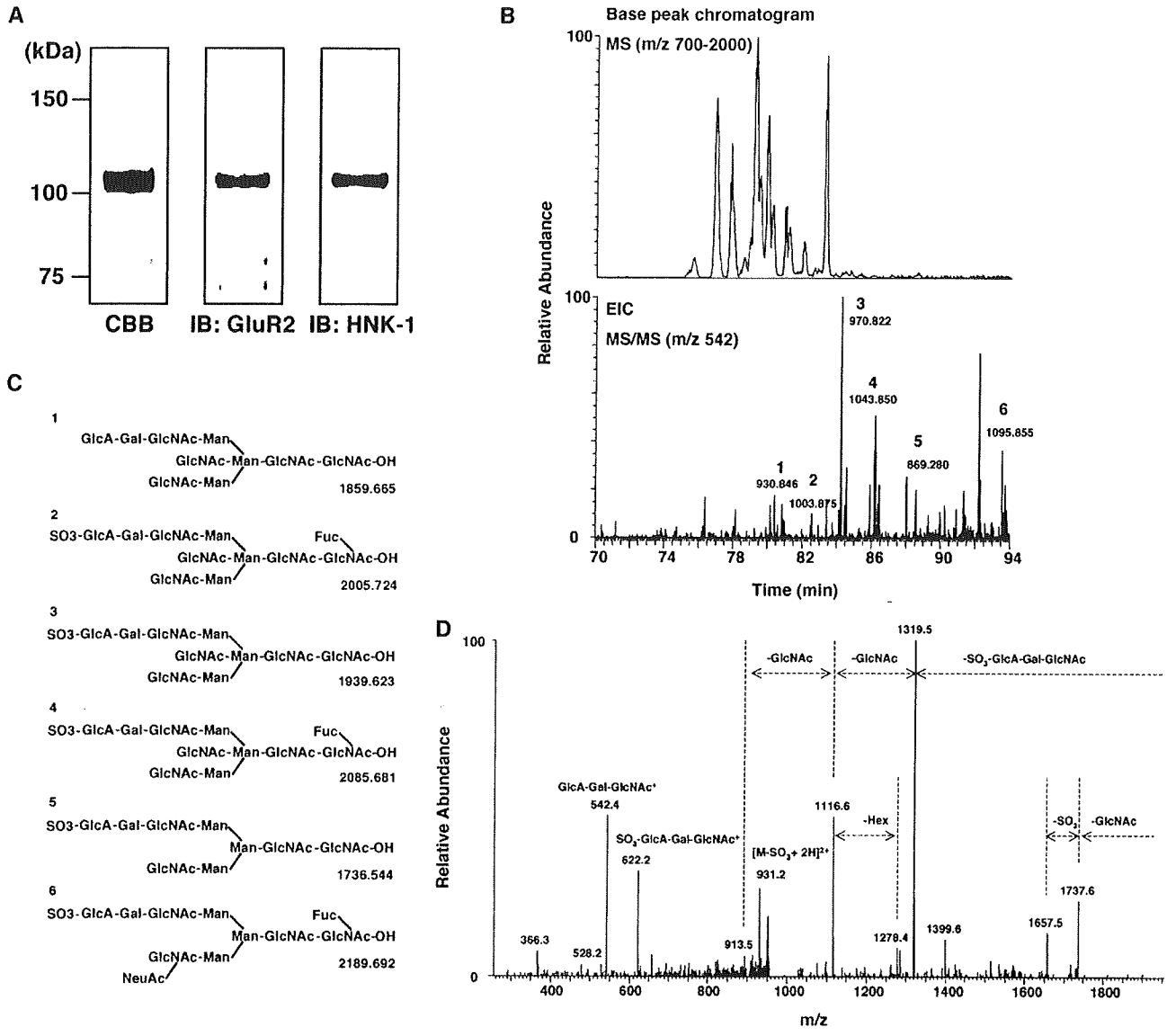


FIGURE 3. **LC/MS/MS of *N*-linked oligosaccharides on GluR2.** *A*, GluR2 from the P2 fraction of hippocampi was purified using an anti-GluR2 antibody column. The purified GluR2 was digested with *N*-glycosidase F, and the extracted *N*-linked oligosaccharides were analyzed by LC/MS/MS. *B*, peak chromatogram obtained by a full MS scan (*m/z* 700–2000) of borohydride-reduced *N*-linked oligosaccharides released from the gel-separated GluR2 (*upper panel*). Extracted ion chromatogram (*m/z* 542) was from a data-dependent MS/MS scan, and *m/z* values of precursor ions were obtained by FT-ICR MS (*lower panel*). *C*, deduced structures of *peaks 1–6* and their theoretical masses as shown in *B*. *D*, MS/MS spectrum of peak 3 as shown in *B*.

Fig. 2, these data show that HNK-1 is actually expressed on *N*-glycans of GluR2 in the brain.

*HNK-1 Glyco-epitope on GluR2 Regulates the Endocytosis of GluR2 in Hippocampal Neurons*—Numerous recent studies have strongly suggested that the mechanism underlying activity-dependent synaptic plasticity is related to the redistribution of GluR2 between intracellular components and the synaptic membrane (15). GluR2 is internalized by clathrin-dependent endocytosis, and two distinct types of GluR2 endocytosis are known, constitutive (under basal conditions) and regulated endocytosis (under stimulation by a reagent such as AMPA, *N*-methyl-D-aspartic acid, and insulin) (29). Moreover, we revealed that HNK-1 is specifically expressed on GluR2 (Fig. 2) and that loss of HNK-1 in the brain impairs the synaptic plasticity (8). Taken together, we hypothesized that HNK-1 expression on GluR2 regulates its intracellular distribution. To evaluate the influence of HNK-1 epitope on GluR2 endocytosis, we performed a fluorescence-based internalization assay (30) using hippocampal neurons derived from wild-type or GlcAT-P-deficient mice. In this assay, the surface GluR2 subunits on living neurons at 18 days *in vitro* were labeled with 10 $\mu$g/ml antibody against the extracellular epitope of GluR2, and then antibody-labeled neurons were incubated for 20 min at 37 °C to allow endocytosis either in the absence or presence of 100 $\mu$M AMPA to determine constitutive or regulated GluR2 endocytosis, respectively. The antibody-labeled GluR2 remaining on the cell surface and the GluR2 internalized into intracellular vesicles were independently immunostained under nonperme-

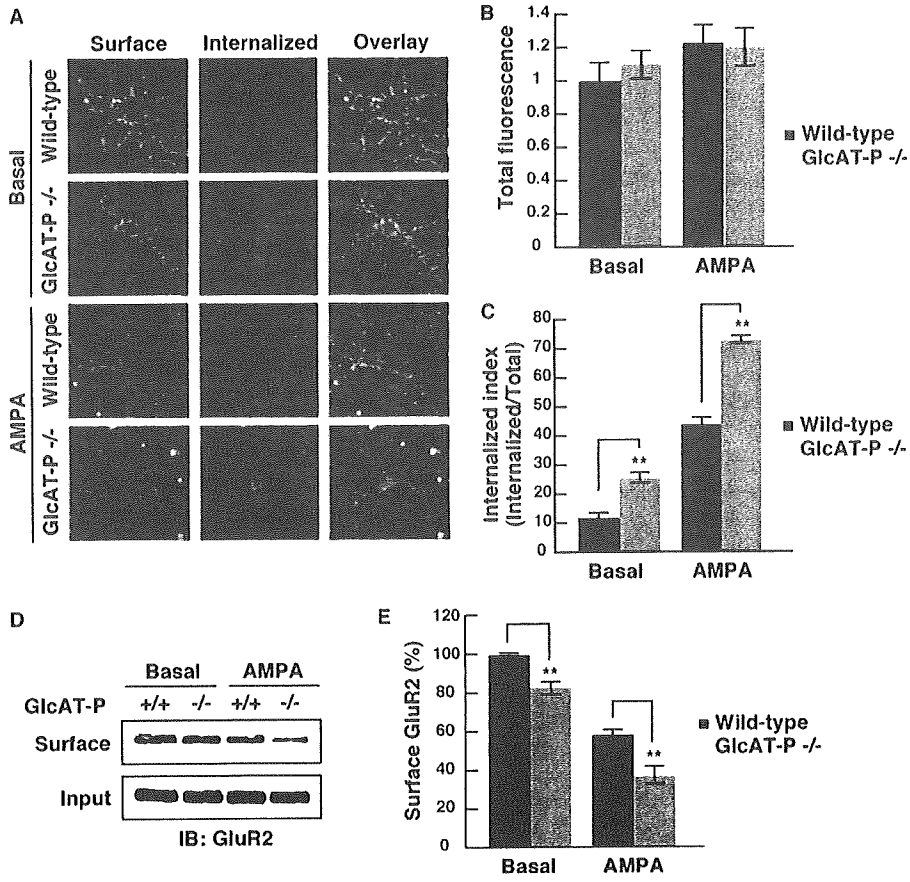


FIGURE 4. **Intracellular and surface GluR2 under basal and AMPA-stimulated conditions in cultured hippocampal neurons.** *A*, representative images of neurons stained for surface and internalized GluR2, following 20 min of incubation in conditioned medium or incubation in conditioned medium containing 100 $\mu$M AMPA plus 50 $\mu$M D-2-amino-5-phosphonopentanoic acid. *B*, quantification of total GluR2 fluorescence (surface + internalized GluR2) normalized to the value of GluR2 in wild-type neurons under the basal conditions ($n$ = 17–26 for each condition). *C*, quantification of intracellular accumulation of GluR2, measured as the ratio of internalized fluorescence/total fluorescence (internalization index). **, $p < 0.01$ (two-tailed $t$ test). *D*, biotinylation assay of surface GluR2. Under basal or AMPA-stimulated conditions, the cell surface proteins on hippocampal neurons were biotinylated, and biotinylated GluR2 was precipitated with streptavidin beads and immunoblotted (*IB*) with anti-GluR2 antibody. *E*, quantification of surface GluR2. The amount of surface GluR2 as shown in *D* was measured by band intensity and normalized to inputs, respectively ($n$ = 3). **, $p < 0.01$ (two-tailed $t$ test). *Error bars* indicate S.E.

abilizing and permeabilizing conditions, respectively (Fig. 4*A*). The total fluorescence (surface and internalized fluorescence) of all four conditions was unchanged (Fig. 4*B*). The "internalization index" represents the ratio of internalized fluorescence/total fluorescence and was compared with wild-type neurons under basal and AMPA-stimulated conditions (Fig. 4*C*). Under basal conditions, GluR2 in GlcAT-P-deficient neurons showed a higher degree of intracellular accumulation than GluR2 in wild-type neurons (wild-type, 11.7 ± 1.35; GlcAT-P$^{-/-}$, 25.1 ± 1.87; **, $p < 0.01$) (Fig. 4, *A* and *C*). Under AMPA-stimulated conditions, the amount of intracellular GluR2 in GlcAT-P-deficient neurons was more greatly increased than that in wild-type neurons (wild type, 43.7 ± 2.09; GlcAT-P$^{-/-}$, 72.5 ± 1.49; **, $p < 0.01$). Next we performed a cell surface biotinylation assay to test the surface levels of GluR2 in cultured hippocampal neurons. The amount of surface GluR2 in GlcAT-P-deficient neurons was slightly decreased to 82.5 ± 3.5% of wild type under the basal conditions (**, $p < 0.01$) (Fig. 4, *D* and *E*). After AMPA treatment, the surface expression levels of GluR2 both in wild-type and GlcAT-P-deficient neurons were decreased, but the surface expression in GlcAT-P-deficient neurons was decreased more than that in wild type (wild type, 58.1 ± 2.6%; GlcAT-P$^{-/-}$, 35.5 ± 4.5; **, $p < 0.01$). These results from two independent experiments were consistent with each other and revealed that GluR2 in GlcAT-P-deficient neurons showed facilitated endocytosis or instability on the cell surface under both basal and stimulated conditions.

*HNK-1 Epitope Is Involved in the Interaction between GluR2 and N-cadherin*—A recent report has shown that the extracellular N-terminal domain of GluR2 interacts with N-cadherin and that the interaction plays important roles in the surface diffusion of GluR2 on neuronal membranes (31). It was also reported that the association between GluRs and N-cadherin regulates the trafficking and surface expression of AMPA receptors (32). As described above, it seems that HNK-1 deficiency leads to destabilization of GluR2 on the neuronal cell surface. To determine whether the HNK-1 epitope on the N-terminal domain is involved in the interaction of GluR2 with N-cadherin, we compared the amount of N-cadherin associated with GluR2 between the wild-type and GlcAT-P-deficient mice by means of a co-immunoprecipitation experiment. In brief, the P2 fraction prepared from hippocampi was treated with DTSSP for protein cross-linking and then solubilized with 1% Triton X-100. The GluR2-containing complex was immunoprecipitated from the Triton X-100-soluble and -insoluble fractions using anti-GluR2 antibody, and the cross-linking was then reversed and analyzed by immunoblot analysis with antibodies against GluR2 and N-cadherin, respectively. Because of the existence of synaptophysin and PSD-95 (Fig. 5*A*, *input*, *middle* and *lower panels*), we refer to the soluble and insoluble fractions as the pre- and postsynaptic protein-rich fractions, respectively. In the presynaptic protein-rich fraction (soluble fraction), the interaction between GluR2 and N-cadherin was hardly detected (Fig. 5*A*). GluR2 interacted with N-cadherin in the postsynaptic protein-rich fraction (insoluble fraction) from wild-type and GlcAT-P-deficient mice (Fig. 5*A*). However, the amount of N-cadherin co-immunoprecipitated with GluR2 in GlcAT-P-deficient mice significantly decreased to 64.8 ± 6.4% that in wild-type mice

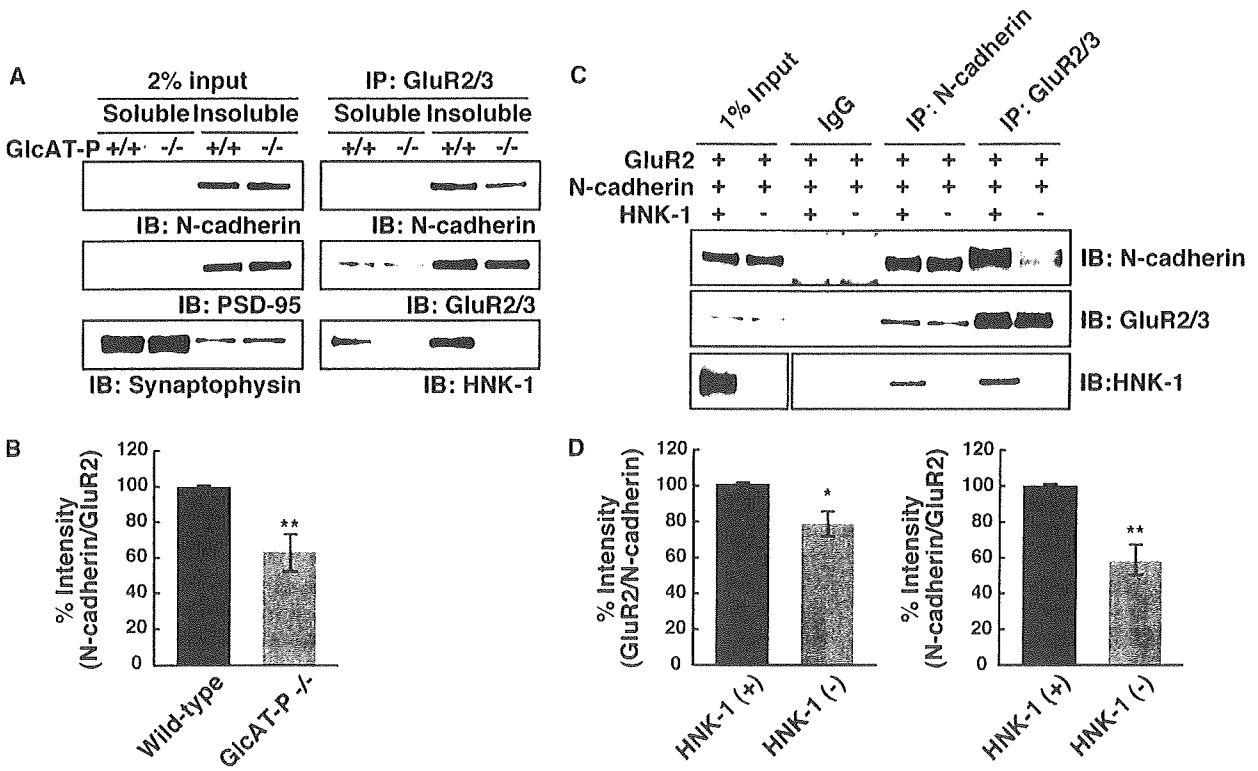


FIGURE 5. **HNK-1 glyco-epitope on GluR2 enhances the interaction with N-cadherin.** *A*, P2 fractions from hippocampi of wild-type and GlcAT-P$^{-/-}$ mice at P14 were cross-linked with DTSSP and then solubilized with 1% Triton X-100. Both soluble and insoluble fractions were immunoprecipitated (*IP*) with anti-GluR2/3 antibodies, and the immunoprecipitate complexes were immunoblotted (*IB*) for GluR2/3, N-cadherin, and HNK-1. Note that the fractions that contain synaptophysin or PSD-95 are the pre- and postsynaptic protein-rich fractions, respectively. *B*, quantification of N-cadherin co-immunoprecipitated with GluR2 in *A*. N-cadherin associated with GluR2 was normalized to immunoprecipitated GluR2 ($n = 5$). **, $p < 0.01$ (two-tailed *t* test). *C*, immunoprecipitation analysis of GluR2 interacting with N-cadherin in HEK 293 cells. HEK 293 cells were overexpressed with GluR2 and N-cadherin in the presence or absence of HNK-1-synthesizing enzymes (GlcAT-P and HNK-1ST), as indicated. After cross-linking with DTSSP, GluR2/3 or N-cadherin was immunoprecipitated. *D*, quantification of GluR2 associated with N-cadherin (*left panel*) and N-cadherin associated with GluR2 (*right panel*) in *C*. The results were normalized by immunoprecipitated N-cadherin ($n = 3$). *, $p < 0.05$; **, $p < 0.01$ (two-tailed *t* test). *Error bars* indicate S.E.

(Fig. 5*B*, **, $p < 0.01$), although the amounts of total N-cadherin and immunoprecipitated GluR2 exhibited no difference between wild-type and GlcAT-P-deficient mice. This result indicates that HNK-1 epitope enhances the interaction between GluR2 and N-cadherin at the postsynaptic membranes. To further corroborate this, N-cadherin and GluR2 expression plasmids were co-transfected into HEK 293 cells in the presence or absence of a plasmid containing HNK-1-synthesizing enzymes (GlcAT-P and HNK-1ST) for the production of GluR2 with or without the HNK-1 epitope. In both HNK-1-positive and -negative cells, the GluR2-N-cadherin interaction was detected (Fig. 5*C*). In the HNK-1-negative cells, the amount of N-cadherin co-immunoprecipitated with GluR2 decreased to 58.3 ± 8.4% (**, $p < 0.01$) that in the HNK-1-positive cells (Fig. 5, *C* and *D*), and in a reverse experiment, the amount of GluR2 co-immunoprecipitated with N-cadherin was reduced to 78.4 ± 6.9% (*, $p < 0.05$) that in the HNK-1-positive cells (Fig. 5, *C* and *D*). These results indicate that HNK-1 epitope enhances the physical interaction of GluR2 with N-cadherin.

*HNK-1 Glyco-epitope Enhances the Surface Expression of GluR2 in an N-cadherin-dependent and -independent Manner*—To corroborate that the interaction between GluR2 and N-cadherin modulated by HNK-1 epitope has an effect on the surface expression of GluR2, we transiently expressed GluR2 and N-cadherin into CHO cells and performed a cell surface biotinylation assay. Unlike HEK 293 cells, CHO cells did not express endogenous N-cadherin. Co-expression of N-cadherin slightly increased the surface expression of GluR2 (119.1 ± 8.7%) (Fig. 6, *A* and *B*). To examine the effect of HNK-1 on the surface expression of GluR2, we next expressed the HNK-1 epitope on GluR2 by GlcAT-P and HNK-1ST in the absence or presence of N-cadherin. The expression of HNK-1 increased the surface level of GluR2 even in the absence of N-cadherin (137.4 ± 10.1%), but the effect of the HNK-1 was more obvious in the presence of N-cadherin (238.2 ± 34.5%). Taken together, these results indicated that the surface stability of GluR2 was enhanced by HNK-1 in both an N-cadherin-dependent and -independent manner.

## DISCUSSION

In the nervous system, various types of cells recognize and interact with each other to form a precise neural network. During this process, carbohydrates expressed on proteins, especially cell surface and secreted proteins, give rise to the structural and functional diversities of carrier proteins. Among them, HNK-1 glyco-epitope is mainly expressed on immunoglobulin family cell adhesion molecules (NCAM, L1, P0, etc.)

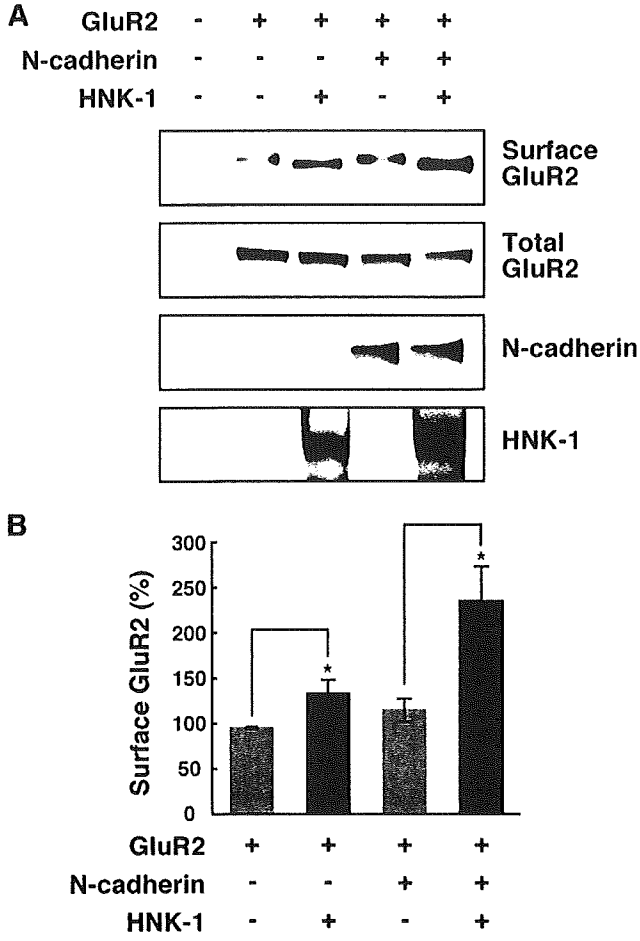


FIGURE 6. **HNK-1 glyco-epitope enhances the surface expression of GluR2 in an N-cadherin-dependent and -independent manner.** *A*, CHO cells were overexpressed with GluR2, N-cadherin, and HNK-1-synthesizing enzymes as indicated. The cell surface proteins on CHO cells were biotinylated, and biotinylated GluR2 molecules were precipitated with streptavidin beads and immunoblotted with anti-GluR2 antibody (*Surface GluR2*). The overexpressed GluR2 (*Total GluR2*) or N-cadherin in each cell lysate was almost equivalent. The HNK-1 epitope was expressed on GluR2 when GlcAT-P and HNK-1ST were overexpressed. *B*, quantification of the surface expression of GluR2 in *A*. The intensity of surface GluR2 was normalized to total GluR2, and the *bar graph* shows the percentages compared with control cells ($n = 5$). *, $p < 0.05$ (two-tailed *t* test). *Error bars* indicate S.E.

and extracellular matrix proteins (tenascin-R, phosphacan, etc.) (12, 33). Thus far, most previous studies have focused on the adhesive and morphological functions of HNK-1 epitope on these molecules and have shown its relationship to neural crest cell migration, neuron to glial cell adhesion, and the outgrowth of astrocytic processes (3). From the aspect of synaptic plasticity, the HNK-1 epitope carried by tenascin-R has been well characterized. Tenascin-R is highly present in the perineuronal nets surrounding parvalbumin-positive inhibitory interneurons (34, 35). It is proposed that HNK-1 epitope on tenascin-R is involved in the regulation of perisomatic inhibition of CA1 pyramidal neurons via reduction of evoked γ-aminobutyric acid release, resulting in the reduction of LTP in CA1 pyramidal neurons (12, 36). In this study, we report that the HNK-1 epitope is expressed at excitatory postsynaptic sites on hippocampal pyramidal neurons (Fig. 1). We first identified the neurotransmitter receptor subunit GluR2 as a novel HNK-1 carrier molecule (Figs. 2 and 3). HNK-1 regulates the synaptic functions of GluR2 by modulating the surface expression of GluR2 (Figs. 4 and 6). This study provides new aspects for understanding the role of HNK-1 glyco-epitope in synaptic plasticity.

In mature pyramidal neurons, GluR1 and GluR2 are predominantly expressed, and the great majority of AMPA receptors contain GluR2 subunits. In particular, it is considered that GluR2 subunit plays pivotal roles in receptor assembly and trafficking (15, 37). GluR1 and GluR2 are synthesized and assembled into tetrameric AMPA receptor complexes in the endoplasmic reticulum. After their assembly, the HNK-1 on GluR2 is synthesized by GlcAT-P and HNK-1ST in the Golgi apparatus. GluR2 has four *N*-glycosylation sites in its extracellular N-terminal domain, and all of them are conserved between GluR2 and GluR1 (16). Interestingly, although GluR1 and GluR2 have high homology with respect to their amino acid sequence and common biosynthesis pathway, HNK-1 is selectively expressed on GluR2 but not on GluR1. This result suggests that HNK-1 regulates the specific function of GluR2 and influences excitatory synaptic transmissions.

It has been widely demonstrated that GluR2 interacts with its intracellular and extracellular partners, and these interactions control AMPA receptor functions such as receptor trafficking and stabilization on the cell surface (38). Glutamate receptor interacting protein/AMPA-binding protein and protein interacting with protein kinase C-1 are partners that associate with the PDZ domain in the intracellular C-terminal tail of GluR2. The interactions of glutamate receptor interacting protein/AMPA-binding protein and protein interacting with protein kinase C-1 with GluR2 depend on the phosphorylation status of the C terminus of GluR2 (including Ser-880 and Tyr-876 residues) (39–41). Another intracellular partner, *N*-ethylmaleimide-sensitive fusion protein, binds to the C-terminal membrane-proximal site of GluR2 and plays important roles in the insertion of AMPA receptors into postsynaptic membranes (42, 43). This *N*-ethylmaleimide-sensitive fusion protein-binding site overlaps with the binding site of AP2, which is an adaptor protein for cargo in clathrin-dependent endocytosis (30, 44). We examined the interactions of GluR2 with these proteins, but there was no apparent difference between wild-type and GlcAT-P-deficient mice (data not shown). As for the extracellular N-terminal domain of GluR2, there are few reports about its functions and interactions with its partners. Passafaro *et al.* (45) demonstrated that the overexpression of the GluR2 N-terminal domain exhibited an increase in the number of functional synapses and enlargement of spine heads in cultured hippocampal neurons. A recent study (31) showed that the interaction with N-cadherin is needed for the synapse (spine) promotion activity and stabilization of GluR2 on the neuronal surface. In this study, the absence of the HNK-1 epitope on GluR2 reduced its interaction with N-cadherin *in vivo* and *in vitro* (Fig. 5). Corresponding to this, we observed the abnormal dendritic spine morphogenesis in early postnatal GlcAT-P-deficient mice and in cultured hippocampal neurons.[4] During

[4] I. Morita, S. Kakuda, Y. Takeuchi, T. Kawasaki, and S. Oka, unpublished data.

synaptogenesis (at postnatal day 14), most pyramidal neurons in wild-type mice possessed mature spines with mushroom-like heads, but the majority of dendritic protrusions were long and thin immature filopodia-like spines in GlcAT-P-deficient mice. These data led us to suggest that HNK-1 on GluR2 controls not only AMPA receptor trafficking but also spine morphogenesis. However, HNK-1 is widely expressed on a series of cell adhesion molecules and extracellular molecules other than GluR2 (Fig. 1). As the HNK-1 on these molecules has almost completely disappeared in GlcAT-P-deficient mice (Fig. 1), it is difficult to rule out the involvement of the HNK-1 on other molecules in spine morphology. Although we reveal in this study that HNK-1 on GluR2 is probably involved in synaptic plasticity by regulating its cell surface expression level through its interaction with N-cadherin *in vivo*, further investigation is necessary to clarify the precise molecular mechanisms of spine formation and synaptic plasticity regulated by the HNK-1 glyco-epitope.

*Acknowledgment—We thank Dr. A. Ikeda (Kyoto University) for valuable discussion and technical advice.*

## REFERENCES


1. Morita, I., Kizuka, Y., Kakuda, S., and Oka, S. (2008) *J. Biochem.* **143,** 719–724
2. Künemund, V., Jungalwala, F. B., Fischer, G., Chou, D. K., Keilhauer, G., and Schachner, M. (1988) *J. Cell Biol.* **106,** 213–223
3. Bronner-Fraser, M. (1987) *Dev. Biol.* **123,** 321–331
4. Martini, R., Xin, Y., Schmitz, B., and Schachner, M. (1992) *Eur. J. Neurosci.* **4,** 628–639
5. Terayama, K., Oka, S., Seiki, T., Miki, Y., Nakamura, A., Kozutsumi, Y., Takio, K., and Kawasaki, T. (1997) *Proc. Natl. Acad. Sci. U.S.A.* **94,** 6093–6098
6. Seiki, T., Oka, S., Terayama, K., Imiya, K., and Kawasaki, T. (1999) *Biochem. Biophys. Res. Commun.* **255,** 182–187
7. Bakker, H., Friedmann, I., Oka, S., Kawasaki, T., Nifant'ev, N., Schachner, M., and Mantei, N. (1997) *J. Biol. Chem.* **272,** 29942–29946
8. Rabouille, C., Hui, N., Hunte, F., Kieckbusch, R., Berger, E. G., Warren, G., and Nilsson, T. (1995) *J. Cell Sci.* **108,** 1617–1627
9. Yamamoto, S., Oka, S., Inoue, M., Shimuta, M., Manabe, T., Takahashi, H., Miyamoto, M., Asano, M., Sakagami, J., Sudo, K., Iwakura, Y., Ono, K., and Kawasaki, T. (2002) *J. Biol. Chem.* **277,** 27227–27231
10. Strekalova, T., Wotjak, C. T., and Schachner, M. (2001) *Mol. Cell. Neurosci.* **17,** 1102–1113
11. Pradel, G., Schachner, M., and Schmidt, R. (1999) *J. Neurobiol.* **39,** 197–206
12. Saghatelyan, A. K., Gorissen, S., Albert, M., Hertlein, B., Schachner, M., and Dityatev, A. (2000) *Eur. J. Neurosci.* **12,** 3331–3342
13. Yoshihara, T., Sugihara, K., Kizuka, Y., Oka, S., and Asano, M. (2009) *J. Biol. Chem.* **284,** 12550–12561
14. Derkach, V. A., Oh, M. C., Guire, E. S., and Soderling, T. R. (2007) *Nat. Rev. Neurosci.* **8,** 101–113
15. Isaac, J. T., Ashby, M., and McBain, C. J. (2007) *Neuron* **54,** 859–871
16. Pasternack, A., Coleman, S. K., Féthière, J., Madden, D. R., LeCaer, J. P., Rossier, J., Pasternack, M., and Keinänen, K. (2003) *J. Neurochem.* **84,** 1184–1192
17. Hall, R. A., Hansen, A., Andersen, P. H., and Soderling, T. R. (1997) *J. Neurochem.* **68,** 625–630
18. Standley, S., Tocco, G., Wagle, N., and Baudry, M. (1998) *J. Neurochem.* **70,** 2434–2445
19. Everts, I., Villmann, C., and Hollmann, M. (1997) *Mol. Pharmacol.* **52,** 861–873
20. Maruo, K., Nagata, T., Yamamoto, S., Nagai, K., Yajima, Y., Maruo, S., and Nishizaki, T. (2003) *Brain Res.* **977,** 294–297
21. Sakimura, K., Bujo, H., Kushiya, E., Araki, K., Yamazaki, M., Yamazaki, M., Meguro, H., Warashina, A., Numa, S., and Mishina, M. (1990) *FEBS Lett.* **272,** 73–80
22. Kizuka, Y., Matsui, T., Takematsu, H., Kozutsumi, Y., Kawasaki, T., and Oka, S. (2006) *J. Biol. Chem.* **281,** 13644–13651
23. Uemura, K., Kihara, T., Kuzuya, A., Okawa, K., Nishimoto, T., Ninomiya, H., Sugimoto, H., Kinoshita, A., and Shimohama, S. (2006) *Neurosci. Lett.* **402,** 278–283
24. Nakamura, M., Sato, K., Fukaya, M., Araishi, K., Aiba, A., Kano, M., and Watanabe, M. (2004) *Eur. J. Neurosci.* **20,** 2929–2944
25. Kizuka, Y., Kobayashi, K., Kakuda, S., Nakajima, Y., Itoh, S., Kawasaki, N., and Oka, S. (2008) *Glycobiology* **18,** 331–338
26. Laemmli, U. K. (1970) *Nature* **227,** 680–685
27. Kikuchi, M., Hatano, N., Yokota, S., Shimozawa, N., Imanaka, T., and Taniguchi, H. (2004) *J. Biol. Chem.* **279,** 421–428
28. Küster, B., Wheeler, S. F., Hunter, A. P., Dwek, R. A., and Harvey, D. J. (1997) *Anal. Biochem.* **250,** 82–101
29. Man, H. Y., Lin, J. W., Ju, W. H., Ahmadian, G., Liu, L., Becker, L. E., Sheng, M., and Wang, Y. T. (2000) *Neuron* **25,** 649–662
30. Lee, S. H., Liu, L., Wang, Y. T., and Sheng, M. (2002) *Neuron* **36,** 661–674
31. Saglietti, L., Dequidt, C., Kamieniarz, K., Rousset, M. C., Valnegri, P., Thoumine, O., Beretta, F., Fagni, L., Choquet, D., Sala, C., Sheng, M., and Passafaro, M. (2007) *Neuron* **54,** 461–477
32. Nuriya, M., and Huganir, R. L. (2006) *J. Neurochem.* **97,** 652–661
33. Liedtke, S., Geyer, H., Wuhrer, M., Geyer, R., Frank, G., Gerardy-Schahn, R., Zähringer, U., and Schachner, M. (2001) *Glycobiology* **11,** 373–384
34. Wintergerst, E. S., Vogt Weisenhorn, D. M., Rathjen, F. G., Riederer, B. M., Lambert, S., and Celio, M. R. (1996) *Neurosci. Lett.* **209,** 173–176
35. Brückner, G., Grosche, J., Schmidt, S., Härtig, W., Margolis, R. U., Delpech, B., Seidenbecher, C. I., Czaniera, R., and Schachner, M. (2000) *J. Comp. Neurol.* **428,** 616–629
36. Dityatev, A., and Schachner, M. (2003) *Nat. Rev. Neurosci.* **4,** 456–468
37. Santos, S. D., Carvalho, A. L., Caldeira, M. V., and Duarte, C. B. (2009) *Neuroscience* **158,** 105–125
38. Bassani, S., Valnegri, P., Beretta, F., and Passafaro, M. (2009) *Neuroscience* **158,** 55–61
39. Matsuda, S., Launey, T., Mikawa, S., and Hirai, H. (2000) *EMBO J.* **19,** 2765–2774
40. Chung, H. J., Xia, J., Scannevin, R. H., Zhang, X., and Huganir, R. L. (2000) *J. Neurosci.* **20,** 7258–7267
41. Chung, H. J., Steinberg, J. P., Huganir, R. L., and Linden, D. J. (2003) *Science* **300,** 1751–1755
42. Nishimune, A., Isaac, J. T., Molnar, E., Noel, J., Nash, S. R., Tagaya, M., Collingridge, G. L., Nakanishi, S., and Henley, J. M. (1998) *Neuron* **21,** 87–97
43. Noel, J., Ralph, G. S., Pickard, L., Williams, J., Molnar, E., Uney, J. B., Collingridge, G. L., and Henley, J. M. (1999) *Neuron* **23,** 365–376
44. Kastning, K., Kukhtina, V., Kittler, J. T., Chen, G., Pechstein, A., Enders, S., Lee, S. H., Sheng, M., Yan, Z., and Haucke, V. (2007) *Proc. Natl. Acad. Sci. U.S.A.* **104,** 2991–2996
45. Passafaro, M., Nakagawa, T., Sala, C., and Sheng, M. (2003) *Nature* **424,** 677–681

**Glycobiology** vol. 19 no. 8 pp. 868–878, 2009
doi:10.1093/glycob/cwp060
Advance Access publication on April 23, 2009

# Regulated expression of the HNK-1 carbohydrate is essential for medaka (Oryzias latipes) embryogenesis

**Daisuke Anzai[2], Yasuhiro Tonoyama[3], Atsushi Ikeda[2], Toshisuke Kawasaki[4], and Shogo Oka[1,3]**

[2]Department of Biological Chemistry, Graduate School of Pharmaceutical Sciences, Kyoto University, Kyoto 606-8501; [3]Department of Biological Chemistry, Human Health Sciences, Graduate School of Medicine, Kyoto University, Kyoto 606-8507; and [4]The Research Center for Glycobiotechnology, Ritsumeikan University, Shiga 525-8577, Japan

*Received on March 13, 2009; revised on April 16, 2009; accepted on April 17, 2009*

**Carbohydrates are known to play essential roles in various biological processes including development. However, it remains largely unknown which carbohydrate structure takes part in each biological event. Here, we examined the roles of the human natural killer-1 (HNK-1) carbohydrate in medaka embryogenesis. We first cloned two medaka glucuronyltransferases, GlcAT-P and GlcAT-S, key enzymes for HNK-1 biosynthesis. Overexpression of these glucuronyltransferases affected morphogenetic processes. In addition, loss-of-function experiments revealed that GlcAT-P is physiologically indispensable for head morphogenesis and GlcAT-P depletion also led to markedly increased apoptosis. However, even when the apoptosis was blocked, abnormal head morphogenesis caused by GlcAT-P depletion was still observed, indicating that apoptosis was not the main cause of the abnormality. Moreover, in situ hybridization analyses indicated that GlcAT-P depletion resulted in the abnormal formation of the nervous system but not in cell specification. These results suggest that tight regulation of HNK-1 expression is essential for proper morphogenesis of medaka embryos.**

*Keywords:* apoptosis/development/glucuronyltransferase/HNK-1 carbohydrate/medaka

## Introduction

Glycosylation is one of the major post-translational modifications frequently found in membrane-targeted and secreted proteins. Glycosyltransferases are the enzymes that transfer a monosaccharide unit to an acceptor molecule, and thus are essential for synthesis of carbohydrate chains. Over the past few decades, a considerable number of studies have been carried out to elucidate the roles of specific carbohydrates in various biological processes through manipulation of glycosyltransferase activities (Lowe and Marth 2003; Ohtsubo and Marth 2006). For example, gene-knockout studies have revealed that each structurally different carbohydrate has a specific function in murine embryogenesis (Metzler et al. 1994). In many cases, the expression profiles of structurally distinct carbohydrates are known to change dramatically during early development, making a subset of carbohydrates extremely specific and useful differentiation markers (Solter and Knowles 1978). Among such differentiation marker carbohydrates, human natural killer-1 (HNK-1) is a carbohydrate specifically expressed in the central nervous system in a developmentally regulated manner (Schwarting et al. 1987; Yoshihara et al. 1991) and has a unique structural feature of the sulfoglucuronyl residue at nonreduced terminus of glycan (Chou et al. 1986; Voshol et al. 1996). Two glycosyltransferases, glucuronyltransferase-P (GlcAT-P) and glucuronyltransferase-S (GlcAT-S), are essential for the biosynthesis of the HNK-1 carbohydrate in vivo (Terayama et al. 1997, 1998; Seiki et al. 1999; Mitsumoto et al. 2000; Yamamoto et al. 2002). The characteristic expression of the HNK-1 carbohydrate is observed in rhombomeres (Kuratani 1991) and migrating neural crest cells (Bronner-Fraser 1986) in developing mouse embryos, and in chick epiblasts as a salt-pepper-like pattern (Canning and Stern 1988). In the case of chick epiblasts, it has been shown that the cells containing the HNK-1 carbohydrate are required for gastrulation (Stern and Canning 1990), indicating that this carbohydrate plays essential roles during embryogenesis. As the HNK-1 carbohydrate is mainly present on cell adhesion molecules and components of the extracellular matrix, it is generally considered to modify the cell–cell and cell–matrix interactions (Saghatelyan et al. 2000; Liedtke et al. 2001). However, the knowledge about the physiological roles of the HNK-1 carbohydrate in early development, especially at the molecular level, remains very much limited. One of the main reasons for this is that early development in the above-mentioned model organisms is mostly inaccessible, as it takes place either in the uterus or inside an opaque eggshell. To circumvent this problem, here we used a teleost fish medaka as a model, as its early development can be observed in detail without a perturbation of natural developmental processes, and micromanipulation, e.g., gene knockdown and overexpression, can be readily carried out.

In this study, we investigated in detail the functions of the HNK-1 carbohydrate in medaka embryonic development. We first cloned cDNAs encoding two medaka glucuronyltransferases, GlcAT-P and GlcAT-S, and characterized the expression of these GlcATs along with the HNK-1 carbohydrate during early development. In addition, gain- and loss-of-function analyses revealed that the appropriate expression level of the HNK-1 carbohydrate is essential for proper morphogenesis, especially in the head region.

[1]To whom correspondence should be addressed: Tel:/Fax: +81-75-751-3959; e-mail: shogo@hs.med.kyoto-u.ac.jp

 

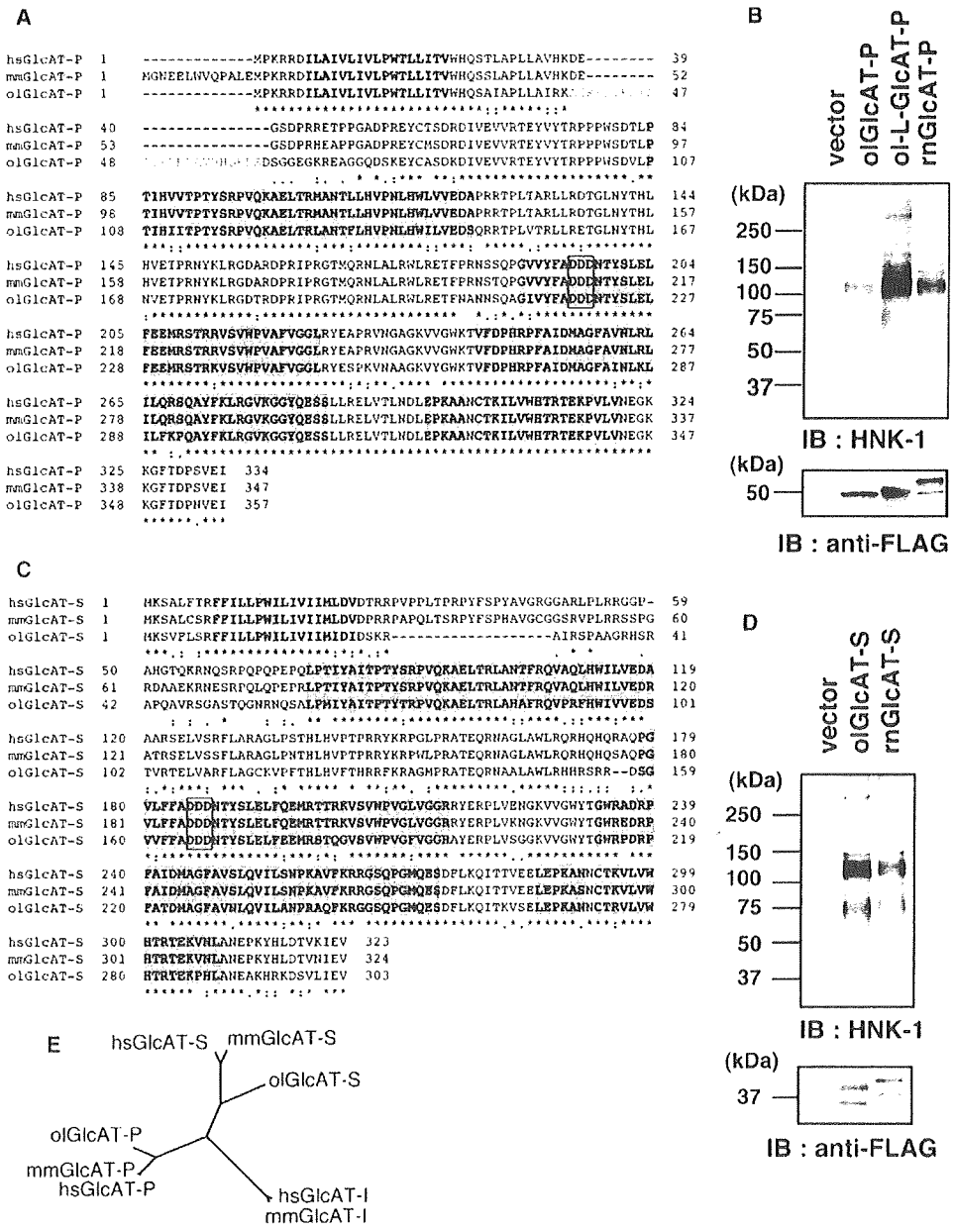


**Fig. 1.** Identification and characterization of medaka GlcAT-P and GlcAT-S. (**A, C**) Multiple alignment of amino acid sequences of medaka (ol), human (hs), and mouse (mm) GlcAT-P and GlcAT-S. Motifs conserved in all the three species are indicated by asterisks. Blue, yellow, pink, and purple boxes indicate the transmembrane region, potential *N*-glycosylation sites, residues defining the acceptor substrate specificity and glutamate residue at active site, respectively. Green boxes indicate four highly conserved motifs among species, designated as motifs I–IV. Open box in red indicates DXD motif conserved in most glycosyltransferases. (**B, D**) Immunoblot analysis for the HNK-1 carbohydrate and GlcATs expression. FLAG-tagged medaka or rat (rn) GlcATs were expressed in COS-1 cells, and the cell lysates were prepared and analyzed by immunoblot using anti-HNK-1 and anti-FLAG antibodies. (**E**) Unrooted phylogenetic tree analysis of GlcATs from the three species.

## Results

### *Cloning and characterization of medaka glucuronyltransferases required for the biosynthesis of the HNK-1 carbohydrate*

As an initial step to determine the roles of the HNK-1 carbohydrate in medaka embryogenesis, we first isolated cDNAs encoding the glucuronyltransferase, a rate-limiting enzyme for the biosynthesis of the HNK-1 carbohydrate. To this end, RT-PCR was carried out using degenerate primers corresponding to conserved amino acid sequences among GlcATs of human, mouse, and fugu origin. This led to the identification of cDNAs encoding a partial protein exhibiting sequence similarity to vertebrate GlcATs. We then performed 5′- and 3′-RACE

and finally acquired medaka GlcAT-P and GlcAT-S cDNAs encoding full length (Figure 1A and C). For GlcAT-P, we cloned the cDNAs of two distinct sequences designated as *L-GlcAT-P* (longer clone; accession number AB252648) and *GlcAT-P* (shorter clone; AB252647). We identified single cDNA clone for GlcAT-S (AB252649). The open reading frames of the *L-GlcAT-P*, *GlcAT-P*, and *GlcAT-S* cDNA comprise 1074, 1002, and 912 base pairs, encoding proteins of 358, 334, and 304 amino acids, respectively. According to the genomic sequence information acquired from the Medaka Ensembl Genome Database, two isoforms of *GlcAT-P* are generated through alternative splicing, in which an exon encoding a 24 amino acids stretch is only included in the *L-GlcAT-P* mRNA (Figure 1A, red letters). The medaka *GlcAT-P* and *GlcAT-S* are predicted to contain four exons, and the extra exon included in *L-GlcAT-P* is located between exons 1 and 2 of *GlcAT-P* (denoted as exon 1′ in Figure 4A). *L-GlcAT-P*, *GlcAT-P*, and *GlcAT-S* exhibited 80%, 85%, and 67% amino acid identity to the human ortholog of the respective enzymes. Hydropathy analysis of the deduced amino acid sequences suggested that medaka GlcATs have a single transmembrane region (Figure 1A and C, blue boxes) with type II transmembrane orientation, which is a common feature of most mammalian glycosyltransferases. Medaka GlcAT-Ps and GlcAT-S contain four domains, designated as motifs I–IV, which are highly conserved in GlcATs of various species (Figure 1A and C, green boxes). We previously reported that in human GlcATs orthologs, Glu284 in GlcAT-P and Glu273 in GlcAT-S are the active sites (Figure 1A and C, purple boxes), and Phe245 in GlcAT-P and Trp234 in GlcAT-S define the acceptor substrate specificities (Figure 1A and C, red boxes) (Kakuda et al. 2004; Shiba et al. 2006). These residues are also precisely conserved in medaka GlcATs. In addition, medaka GlcATs contain a DXD motif, which is conserved widely in UDP-sugar-dependent glycosyltransferases (Figure 1A and C, red open boxes) (Negishi et al. 2003). Moreover, there are potential *N*-glycosylation sites (three sites for GlcAT-Ps and two for GlcAT-S) which are also found in mammalian GlcATs (Figure 1A and C, yellow boxes) (Terayama et al. 1997; Seiki et al. 1999). These structural features indicate that medaka GlcAT-Ps and GlcAT-S cDNAs obtained here encode true orthologs of mammalian GlcAT-P and GlcAT-S, respectively. This notion was supported by the phylogenetic analysis (Figure 1E), which confirmed that medaka GlcAT-P and GlcAT-S are more similar to the respective GlcATs of human and mouse origin, but not to GlcAT-I, which is another β-1,3-glucuronyltransferase necessary for the synthesis of glycosaminoglycans (Kitagawa et al. 1998). Next, we measured the glucuronyltransferase activity of the proteins encoded by the cloned medaka GlcATs. For this purpose, we transfected the expression vectors for each cDNA into COS-1 cells, followed by immunoblot analysis of the cell lysates using anti-HNK-1 antibodies. In agreement with our previous observation (Terayama et al. 1997; Seiki et al. 1999), transfection of rat GlcATs cDNA into COS-1 cells resulted in the appearance of immunoreactive bands corresponding to from 70 kDa to over 200 kDa, while mock-transfected cells showed no immunoreactivity (Figure 1B and D). The cells transfected each medaka GlcATs also showed a similar profile of immunoreactive bands (Figure 1B and D), suggesting that these cDNAs encode proteins with glucuronyltransferase activity in the cells. Together, these observations suggested that the three newly cloned medaka GlcATs are true orthologs of mammalian GlcATs and that each of them encodes

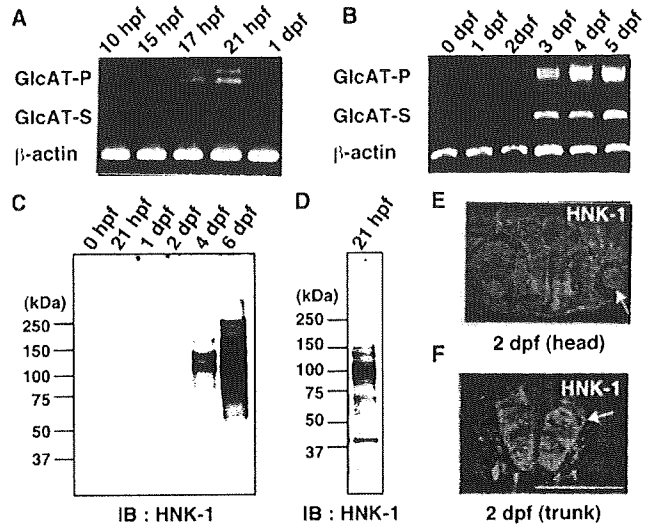


**Fig. 2.** Expression of medaka *GlcATs* and HNK-1 carbohydrate during embryonic development. (A, B) RT-PCR analysis of the two *GlcAT-P* isoforms and *GlcAT-S* along with β-*actin* during medaka embryogenesis. The upper bands in the *GlcAT-P* panels were *L-GlcAT-P* and in the lower *GlcAT-P*. (C, D) Immunoblot analysis for the temporal expression pattern of the HNK-1 carbohydrate during embryonic development. (E, F) Frozen transverse section (10 μm) was prepared from 2 dpf medaka embryos at the head and trunk region, respectively, followed by immunohistochemical staining using anti-HNK-1 antibodies. The HNK-1 carbohydrate is mainly expressed in the brain primordium (red arrow in E), eyes (white arrow in E), neural tube (white arrow in F), and muscle primordium (red arrow in F). Bar, 200 μm.

the enzymatically active proteins required for the biosynthesis of the HNK-1 carbohydrate in the cells.

*Expression pattern of GlcATs and HNK-1 carbohydrate during medaka embryogenesis*

We next examined the temporal expression pattern of *GlcAT-P* and *GlcAT-S* genes. RT-PCR analysis was carried out using RNAs extracted from whole embryos at various developmental stages as a template. When we investigated the expression level during gastrula stages, the expression of *GlcAT-P* was barely detected before 15 h post-fertilization (hpf) and observed at the mid- to late gastrula stages (17–21 hpf), and then had disappeared by 100% epiboly (25 hpf), which is the end of gastrulation (Figure 2A). The *GlcAT-S* expression was not detected during this time window. After the completion of gastrulation and epiboly movements, the expression of both *GlcAT-P* and *GlcAT-S* was first detected at 2 days post-fertilization (dpf) and continued to increase at least up to 5 dpf (Figure 2B). In both time windows, no difference was seen between the expression of longer and shorter splice variants for *GlcAT-P* (appearing as two bands on the gels). Overall, we found that *GlcAT-P* was expressed during gastrulation in a temporally restricted manner, and both *GlcATs* came to be expressed in later stages after 2 dpf. These results suggest that the biosynthesis of the HNK-1 carbohydrate is also briefly upregulated by pulsatile induction of *GlcAT-P* expression during gastrulation and may lead to modification of proteins taking part in the complex processes of gastrulation. We then examined the expression pattern of the HNK-1 carbohydrate during medaka development. Proteins

were extracted from medaka embryos at various stages and immunoblot analysis was performed using anti-HNK-1 antibodies. The bands for proteins carrying the HNK-1 carbohydrate were detected at around 100 kDa as early as 0 hpf (Figure 2C). As descried above, *GlcAT-P* and *GlcAT-S* mRNAs were not detected at this stage, suggesting the presence of some maternally loaded glycoproteins carrying the HNK-1 carbohydrate. During the process of development, additional bands emerged from gastrula stages onward (Figure 2C). As the HNK-1 carbohydrate expression level was very low from gastrulation to 2 dpf, we carried out the control experiment with normal mouse IgM as a primary antibody instead of anti-HNK-1 antibodies to confirm the specificity of these bands. As a result, these bands were not detected in the control experiment (data not shown). We also examined immunoblot analysis using a peroxidase substrate with higher detection sensitivity (see *Material and methods*) for the proteins from 21 hpf embryos (Figure 2D). This revealed that proteins in the around 100–150 kDa range mainly carry the HNK-1 carbohydrate. The results of these and RT-PCR analyses indicate that medaka GlcAT-P, expressed briefly at gastrulation stage, is responsible for the synthesis of the HNK-1 carbohydrate during gastrulation after the mid-blastula transition. We further investigated the localization of the HNK-1 carbohydrate by immunohistochemistry. Frozen sections of medaka embryos at various stages were prepared and stained using anti-HNK-1 antibodies. The expression of the HNK-1 carbohydrate was detected at 2 dpf and was mainly found in the nervous system, e.g., the eye (Figure 2E, white arrow), brain primordium (Figure 2E, red arrow), and neural tube (Figure 2F, white arrow). The muscle primordium was also stained (Figure 2F, red arrow). These results were consistent with previous reports that the HNK-1 carbohydrate is expressed predominantly in the nervous system in mammals (Schwarting et al. 1987; Yoshihara et al. 1991). Although the HNK-1 carbohydrate expression was observed on immunoblot analysis, it was not detected by immunostaining in the embryos before 2 dpf (data not shown). The reason for this is currently unclear, but we believe that the HNK-1 carbohydrate expressed a very low level at the stages earlier than 2 dpf (Sadaghiani and Vielkind 1990). In adult medaka, *GlcATs* and HNK-1 carbohydrate were expressed mainly in the brain, eye, and muscle (data not shown).

### *Proper expression of GlcAT-P and HNK-1 carbohydrate is necessary for medaka development*

The characteristic expression patterns of *GlcAT-P* and HNK-1 carbohydrate in early medaka embryos imply that they may play important roles in these developmental processes. To analyze the possible functions of the HNK-1 carbohydrate during embryogenesis, we performed gain- and loss-of-function analyses of GlcAT-P and GlcAT-S. We first carried out gain-of-function experiments to see if an excess amount of HNK-1 carbohydrate affects the development of medaka embryos. To this end, we injected in vitro synthesized RNA (100–500 pg) encoding GlcAT-P or GlcAT-S fused with a 6× Myc tag into one- to two-cell stage embryos. When observed at 2 dpf, abnormalities in the head regions were detected at the amount of more than 250 pg *GlcAT-P* RNA and 100 pg *GlcAT-S* RNA, respectively. In the case of the embryos injected with 500 pg *GlcAT-P* RNA, the head region was laterally curved from the body axis of the trunk region (Figure 3B). When the same amount of *GlcAT-S*

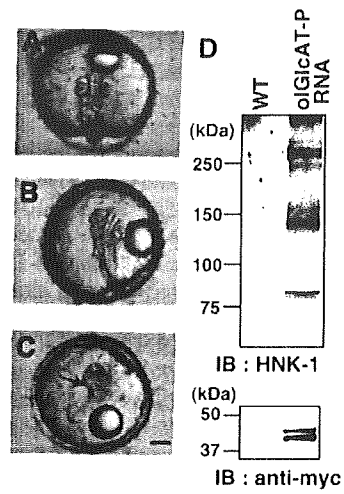


**Fig. 3.** Gain-of-function analysis of GlcAT-P or GlcAT-S in medaka embryos. *GlcATs* mRNA was injected into one- to two-cell stage embryos, and the phenotypes were observed at 2 dpf. Dorsal view, anterior is to the top. (**A**) Non-treated wild-type embryos at 2 dpf. (**B**) The embryos injected with 500 pg *GlcAT-P* RNA showed slight curvature at the head region. (**C**) The embryos injected with 500 pg *GlcAT-S* RNA showed more severe defects such as curved head and shortened body axis. In spite of severe head hypoplasia, these embryos still retained the eye-like structure (arrows). (**D, E**) Immunoblot analysis for the HNK-1 carbohydrate and GlcAT-P expression. Non-treated wild-type and *GlcAT-P* RNA-injected embryos were lysed, and the lysates were analyzed using anti-HNK-1 or anti-Myc antibodies. Bar, 200 μm.

RNA was injected, it resulted in more severe phenotype, i.e., the curvature of the heavily disorganized head region as to the body axis was greater, and the trunk region also appeared to be shorter (Figure 3C). In addition, when 250 pg *GlcAT-S* mRNA was injected, the embryos showed similar phenotypic severity to the embryos injected with 500 pg *GlcAT-P* RNA (data not shown). For investigation of the influence of RNA injection, we injected with 500 pg *EGFP* RNA. As a result, these embryos developed normally (supplementary Figure 1B and C). To make sure that the injection of *GlcATs* RNA indeed led to the ectopic expression of this enzyme and HNK-1 carbohydrate, immunoblot analysis with anti-Myc and anti-HNK-1 antibodies were performed for the lysates obtained from embryos at 2 dpf. We detected the Myc-tagged GlcATs protein and an increased level of the HNK-1 carbohydrate in the injected embryos, suggesting that the injection of *GlcATs* RNA at the one- to two-cell stage actually increased the GlcATs activity, leading to an increase in the HNK-1 carbohydrate as late as 2 dpf (Figure 3D and supplementary Figure 1A). Overall, the overexpression of the GlcATs induced the abnormal development of medaka.

Next, we carried out loss-of-function analyses using antisense morpholino oligonucleotides (MOs) specific to medaka *GlcATs*. MO has been used to inhibit target gene functions with high efficiency and specificity in medaka embryos. In this study, we employed two MOs for *GlcAT-P*, P-MO-1 and P-MO-2 (Figure 4A, red and blue lines, respectively), and one MO for *GlcAT-S*, S-MO (see *Material and methods*). P-MO-1 and S-MO are translation-blocking morpholinos, which bind to the target site including the start codon, while P-MO-2 is a splice-blocking morpholino, which binds to the target region spanning the junction between the third intron and fourth exon (i.e., exon 3)

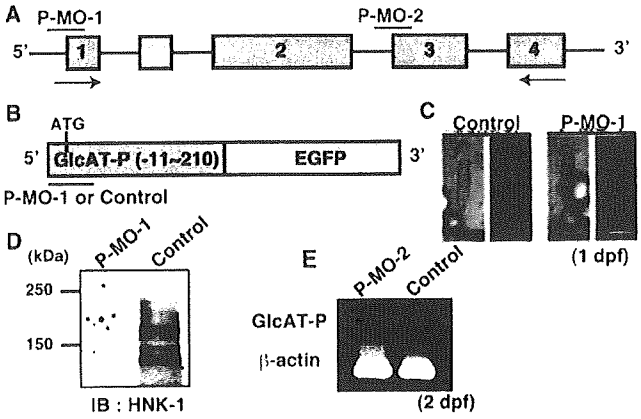


**Fig. 4.** Efficient inhibition of GlcAT-P activity by morpholino oligonucleotides. (**A**) Schematic representation of the exon–intron structures of the *GlcAT-P* gene. The locations of target sequences for P-MO-1 and P-MO-2 were indicated by a red and a blue bar, respectively. Arrows indicate the primers used for RT-PCR in panel E. The box is included only in the longer variant of GlcAT-P. (**B**) Schematic representation of the construct used to confirm the sequence specificity of P-MO-1. The construct contained medaka *GlcAT-P* cDNA including a short segment of the 5′-untranslated region, fused in the frame with the sequence of *EGFP*. (**C**) Dorsal view of embryos at 1 dpf (st. 18), anterior is to the top. Either control MO or P-MO-1 was co-injected with *GlcAT-P-EGFP* RNA at one- to two-cell stage. P-MO-1 significantly inhibited EGFP expression while control MO did not affect EGFP expression. Bar, 200 μm. (**D**) Immunoblot analysis of lysate from P-MO-1- or control MO-injected embryos at 2 dpf. (**E**) RT-PCR analysis revealed that *GlcAT-P* transcripts were reduced by the injection of P-MO-2, but not control MO.

(Figure 4A, line). As a control, MOs containing a five-base mismatch as to the respective target site were used. From the results of these MOs injection, GlcAT-S-depleted embryos developed normally (see Table I), so we analyzed only GlcAT-P-depleted embryos as described below.

To examine the sequence specificity of P-MO-1, we injected P-MO-1 together with RNA encoding *GlcAT-P* fused to *EGFP* into medaka embryos (Figure 4B). When the control MO was co-injected, EGFP fluorescence was clearly observed in the embryonic body of 1 dpf embryos (Figure 4C, left). In contrast, when P-MO-1 was co-injected, fluorescence was not detected, indicating that P-MO-1 blocks the translation of the fusion protein (Figure 4C, right). We also examined sequence specificity of S-MO by co-injection with S-MO and RNA encoding *GlcAT-S* fused to *EGFP* in a similar manner of GlcAT-P. As a result, S-MO also had the sequence specificity against GlcAT-S (data not shown). Moreover, the amount of endogenous proteins carrying the HNK-1 carbohydrate was dramatically reduced in P-MO-1-injected embryos (Figure 4D). Thus, P-MO-1 has competence to inhibit GlcAT-P expression when injected into medaka embryos. On the other hand, MOs targeting exon–intron junctions are known to reduce the amount of the mature transcript and inhibit the function of the target gene product. We injected P-MO-2 or its control MO into medaka embryos and examined the amount of the properly spliced *GlcAT-P* transcript by RT-PCR, finding that P-MO-2 injection led to a marked reduction in the *GlcAT-P* transcript at 2 dpf (Figure 4E). Both P-MO-1 and P-MO-2 are effective in blocking the function of the two isoforms of *GlcAT-Ps*, *L-GlcAT-P* and *GlcAT-P*, as the target sequences of these MOs are located in the common part of these two splice variants (see Figure 4A). These results demonstrated that two independent MOs against *GlcAT-P* designed were useful tools for investigating the physiological function of GlcAT-P during medaka embryonic development.

We thus injected the P-MO-1 or control MO into one- to two-cell stage embryos and observed the external appearance of injected embryos at the 75% epiboly stage (21 hpf) (Figure 5A, B, E, F, J, and K, arrowheads indicate embryonic body edges) and 2 dpf (Figure 5C, D, G, H, I, L, and M). At the 50–75% epiboly stages (mid-gastrula stages), abnormalities of P-MO-1-injected embryos were first observed. Cells around the embryonic body, which was thought to be a presumptive neuroectoderm, were appeared to be darker in color and round shapes compared to control MO-injected ones (compare Figure 5A and B to E and F). The appearance of the dark colored region in the P-MO-1-injected embryos could be due to enhanced apoptosis (compare Figure 6). At this stage, the shorter anterior–posterior length was observed in P-MO-1-injected embryos (Figure 5E). At 2 dpf, control embryos clearly showed two distinct eyes on the sides of the apparent brain structure (Figure 5C) and well-patterned somites (Figure 5D). The injection of P-MO-1 induced a spectrum of phenotypic abnormalities with the head hypoplasia, while the trunk region was less affected (Figure 5G–I). We classified the phenotypes of P-MO-1-injected embryos into two groups according to the severity of the abnormalities. In the mildly affected group (Table I, 23%

**Table I.** Quantification of GlcAT-P- and GlcAT-S-depleted embryo phenotypes

| | | No. (%) of embryos with normal or abnormal phenotypes at 2 dpf | | | | |
|---|---|---|---|---|---|---|
| | | | Abnormal | | | |
| Material injected (ng) | Numbers of embryos examined | Normal | Mild | Severe | Others | Lethal |
| P-MO-1C (5) | 82 | 62 (76) | 0 | 0 | 18 (22) | 2 (2) |
| P-MO-1 (5) | 267 | 69 (26) | 62 (23) | 113 (42) | 0 | 23 (9) |
| P-MO-2C (1) | 43 | 40 (93) | 0 | 0 | 0 | 3 (7) |
| P-MO-2 (1) | 54 | 8 (15) | 20 (37) | 20 (37) | 0 | 6 (11) |
| S-MO-C (5) | 62 | 48 (77) | 0 | 0 | 12 (19) | 2 (3) |
| S-MO (5) | 62 | 52 (84) | 0 | 0 | 7 (11) | 3 (5) |

Embryos were injected control MO with a five-base mismatch or two GlcAT-P and one GlcAT-S specific MO into one- to two-cell stage. P-MO-1 and S-MO are translation blocking morpholinos and P-MO-2 is a splicing blocking morpholino. The phenotypes of P-MO-injected embryos were classified into two groups according to the severity of the abnormalities at 2 dpf. Given is the absolute number of embryos, and the percentages are in parentheses.